CHARACTERIZATION OF Sn_xSe_y / SnO_2-Ni PREPARED BY SPRAY PYROLYSIS FOR PHOTOVOLTAIC APPLICATION

MUGAMBI NELSON

(B.Ed Sci.)

I56/CE/26617/2011

A thesis submitted in partial fulfillment of the requirements for the award of the Degree of Master of Science Physics (Material Science) in the School of Pure and Applied Sciences of Kenyatta University

AUGUST, 2016

DECLARATION

This thesis is my original work and has not been presented for the award of any degree or any other award in any university.

Mugambi Nelson …….. .....

Department of Physics Signature Date

Kenyatta University

P.O BOX 43844-00100

NAIROBI-KENYA

This thesis has been submitted for examination with our approval as University Supervisors

Dr. M. Munji ……. …….

Department of Physics Signature Date

Kenyatta University

P.O BOX 43844-00100

NAIROBI-KENYA

Dr. R.J. Musembi …… …….

Department of Physics Signature Date

University of Nairobi

P.O BOX 30197-00100

NAIROBI-KENYA

DEDICATION

This thesis is dedicated to my beloved wife; Penninah, my children Ryan and Merline, my parents; Lewis and Catherine and my sisters; Doreen, Queensbeth and Josyline. God bless you all.

ACKNOWLEDGEMENTS

I appreciate my supervisors Dr. M Munji Kenyatta University and Dr. Robinson J Musembi University of Nairobi for their valuable advice, interest and motivation they gave me at all time during my research. My success in my research work is as a result of their very able guidance and supervision. I also, express my appreciation to Dr. Walter Njoroge; Kenyatta University and Chairman Physics Department 2011-2015 for availing the facilities for the research work. I also render exceptional gratitude to the administration of Kenyatta University for providing a favorable learning atmosphere.

I also render my wholehearted gratitude to the Kenyatta University Physics laboratory technicians under the headship of the Chief Technician Mr. Fredrick Mudinga especially in providing what I needed from the laboratory. My superior thanks is also directed to Mr. Boniface Muthoka technician Physics Department University of Nairobi-Chiromo campus for his expertize input in the use of the Solar simulator, Four point probe and Spectrophotometer Spec 3700 DUV.

I am also indebted to my colleagues Geoffrey Gitonga Riungu and John Mbae for their input and holding my hand even during my lowest moment of my study. Their motivation kept me moving.

My special thanks also goes to my beloved wife; Penninah, my children Ryan and Merline, my parents; Lewis and Catherine, and my sisters; Doreen, Queensbeth and Josyline for their unlimited love and tolerance throughout my studying period. God be with you all. I am honestly glad for the humble time accorded to me which gave me a chance to concentrate in the research work.

Moreover, I give glory to the Almighty God for his guidance throughout the research time. You accorded me with all that I required which made this work a feat; be glorified.

TABLE OF CONTENTS

LIST OF TABLES

LIST OF FIGURES

ABBREVIATIONS, SYMBOLS AND ACRONYMS

AZO	Aluminum doped Zinc oxide,
AZO/Ni	Nickel capped AZO,
cc/min	Cubic centimeter per minute,
CO	Carbon monoxide,
D	Dopant,
DMS	Diluted magnetic semiconductors,
eV	Electron Volt,
Eg	Energy gap,
FET	Field – effect transistor,
FF	Fill factor,
H_2	Hydrogen gas,
IMO	Molybdenum doped indium oxide,
Isc	Short circuit current,
Mo	Molybdenum,
Ni	Nickel,
n	Refractive index,
Ni-SnO_2	Nickel-doped tin oxide,
NSD	Nozzle-to-substrate distance,

^{o}C	Degrees Celsius,
SnO_2	Tin oxide,
SnSe	Tin selenide,
Ta	Tantalum,
TCO	Transparent conducting oxide,
TM	Transition metal,
VIS–NIR	Visible–near infrared,
Voc	Open circuit voltage,
wt %	Weight percent,
Ω	Ohm,
η	Conversion efficiency,
USP	Ultrasonic Spray Pyrolysis,
PV	Photovoltaic,

ABSTRACT

Nickel doped tin oxide and tin monoselenide thin films were coated using spray pyrolysis. Nickel doped tin oxide Precursor solution was prepared using a 0.05M Tin (II) Chloride ($SnCl_4.2H_2O$) and 0.05M Nickel chloride 6-hydrate ($NiCl_2.6H_2O$) in de-ionized water and then being added in ethanol in the ratio 1:1 to get equal proportions, followed by about 2-3 drops of hydrochloric acid. Doping tin oxide was done using uniform concentration of ($NiCl_2.6H_2O$) of 0-10 %. Precursor solution of tin selenide S_xSe_y was prepared using alcoholic solution consisting of tin chloride $Sncl_2.2H_2O$ and 1,1-dimethl-2-selenourea ($C_3H_8N_2Se$) and then heated while stirring and left for about a week. Samples of (Sn_xSe_y) were made in ratios of 1:0.4 to 1:1.4. Thin films of SnO_2, SnO_2: Ni, Sn_xSe_y and Sn_xSe_y- SnO_2: Ni were deposited on glass substrate using Spray pyrolysis at deposition temperature of 375^oC. The samples of tin selenide were characterized by measuring their optical properties using UV-VIS-NIR spectrophotometer 3700 DUV in the range 280nm to 1200nm and were used to calculate solid state and optical properties namely band gap (E_g), refractive index (n) and absorbance (α). The optical band gap of deposited tin selenide ranged between 1.39-2.23ev. The sample of $Sn:Se_{1.0}$ had the highest absorbance of over 46.26% and lowest transmittance of about 44.3% in the VIS-NIR region. The optical band gap of deposited Nickel doped tin oxide ranged between 3.65-3.75ev. The sample of Nickel doped tin oxide of 2% concentration had the highest transmittance of 86.2% and lowest absorbance of about 5.05% in the VIS-NIR region. These properties are suitable for window and absorber layers for application in photovoltaic cell. The diode characteristics such as short circuit current (I_{sc}) = 1.118mA, open circuit voltage (V_{oc}) = 0.607V, fill factor (FF) = 0.6792 and conversion coefficient (η) = 0.4609 % was obtained for Tin selenide (Sn_xSe_y) and nickel doped tin oxide (SnO_2: Ni) solar cell.

CHAPTER 1

INTRODUCTION

1.1Background to the study

Energy is the main driver in any economy because almost everything is directly or indirectly related to energy. Consumption of energy has steadily raised with sophistication of the world. To nourish human advancement, more electrical energy consumption is anticipated in future (Kuo-Jui, 2010). Consumption of fossil fuels to drive the economy has grown exponentially since industrial revolution causing three primary global problems: environmental pollution, depletion of fossil fuels and climate change (Andreev & Grilikhes, 1997). Solar cells are useful for both space and terrestrial applications and furnish the long-duration power supply for satellites. A solar cell transform sunlight to electricity and can grant consistent power which is virtually non-polluting and at low operating cost. Comparing a solar cell with other energy sources such as geothermal plants and hydroelectric power, it is relatively easy and cost effective to install and use the solar cells (Markvat, 1998). The present growing concern is the venture in Photovoltaic cells which are inexpensive rather than major energy sources (fossil fuels) whose cost is ever increasing. Increase in petroleum prices have been contributed by the increase in demand due to human population causing upward pressure (Pirog, 2005).

The Silicon-based solar cell technology is principally being used in photovoltaic industry. Silicon capability as an absorber material is limited because of its indirect band gap as compared to direct band gap materials (Fahrenbrunch & Bube, 1983). Therefore thicker material of Silicon are required to absorb the equal quantity of light as any thin layer of direct band gap material. The main advantage of thin film solar cells in comparison to silicon solar cells is that less energy is needed for processing, comparatively lower costs of the materials needed thus large scale production is viable (Zainal *et al*., 2011). Hence, PV transformation of

solar energy from low expense solar cells will be a highly vital solution to stock the ever growing energy pressure when conventional source of energy is dwindled in the future (Mohd *et al*., 2011).

SnSe is a group IV-VI semiconductor thin film having a wide range of applications due to its high absorption and suitability for optoelectronic applications because it has a narrow direct band gap energy which is around 1.1eV (Jeewan *et al*., 2005). SnSe also has superior optical transmission in the range of 0.5-20μm capable of improving conductivity and mounting current flow in a p-n junction (Bindu *et al.,* 2004). Solar cell materials which are good absorber layers, should possess the following characteristics: (i) the band gap should lie between 1.0 and 2.0 eV, enabling it to absorb a bigger portion of solar energy; (ii) they should be electrically and chemically stable in either alkaline or acid state; (iii) should be cheap and readily available (Mariappan *et al*., 2010). SnSe thin film comply with these properties.

Tin dioxide (SnO_2) thin film exhibit the best chemical and thermal stabilities. It is also economical to make and has good mechanical durability, but has elevated resistivity. SnO_2 in its pure form has a wide band of approximately 3.7 eV and therefore a better n type semiconductor (Toshiyuki *et al*., 1991). Pure SnO_2 film is inferior electrical conductor that is exceedingly transparent in the visible light. However their poor electrical conductivity can be improved by doping with impurities or controlling the stoichiometry (Suhail *et al*., 2012). Tin based solar cells demonstrate superior optical properties and its alloys exhibit good efficiency solar cell materials (Toshiyuki *et al*., 1991). SnO_2: Ni is a transparent conducting oxide semiconductor suitable for application in photovoltaic cells. It is also a direct band gap energy material having nontoxic constituent materials that are abundantly available on the earth.

Due to their availability and non-toxic characteristics, SnSe and Nickel doped Tin Oxide was used for this research work.

1.2 Statement of the Problem

Conventional energy sources such as crude oil and fossil fuel have negative effects on the environment mainly due to pollution. These effects have necessitated the development of substitute energy. Solar energy has attracted a lot of attention. Silicon based technology has been extensively used in solar cells, but it is very expensive. Therefore, there is need to develop alternative materials for solar cell applications with low cost of production. Various semiconductors have been studied to fabricate thin film semiconductors for the solar cell applications. Sn_XSe_Y thin film studied by Lawrence (2011) looks promising p-type material because it has small band gap and high absorption coefficient. SnO_2: Ni thin film studied by Kuppan (2014) shows a good n type material because of its broad band gap. This research studies the characterization of Sn_xSe_y and SnO_2: Ni thin film materials as a P-N junction in solar cells by varying the deposition parameters.

1.3 Objectives

1.3.1 General Objective

The main objective of the study was to deposit and characterize thin films of Nickel doped Tin Oxide (SnO_2: Ni) and Tin Selenide (Sn_xSe_y) for fabricating a P-N junction for solar cell applications.

1.3.2 Specific Objectives

i. To deposit Sn_xSe_y and SnO_2: Ni thin films at various ratios using spray pyrolysis.
ii. To optically characterize SnO_2: Ni and Sn_xSe_y thin films.
iii. To determine the electrical properties of SnO_2: Ni and Sn_xSe_y thin films using Four point probe method.
iv. To fabricate and characterize Sn_xSe_y-SnO_2: Ni p-n junction solar cell using a solar simulator.

1.4 Rationale of the Study

Fossil fuels like coal, gas and oil mainly causes climate changes and Global warming if they are extensively used. Carbon dioxide, Sulphur and Nitrogen Oxide by products of fossil fuels may bring about acid rain. Therefore it is imperative to switch to energy sources which are efficient, in a sustainable form and clean. Fossil fuels, a major source of energy is depleting fast. This has brought about a crisis. There has been attention in research of alternative energy sources such as nuclear, hydroelectric power, tidal, geothermal power, and solar energy. Photovoltaic technology has facilitated tapping the energy from the sun which is one of the promising clean renewable energy source. Low cost PV devices are required to compete well with other sources of energy. High conversion rates and low cost technologies are the two approaches to achieve this goal. Comparing Silicon and SnSe thin films the latter are efficient absorber layers in solar cell applications. SnO_2: Ni optical properties shows a high transparency in the visible region and doping with Nickel brings about variation. Tin selenide (Sn_xSe_y) and nickel doped tin oxide (SnO_2: Ni) semiconductor have a significant role in devices such as solar cell.

CHAPTER 2

LITERATURE REVIEW

2.1 Solar cells Evolution

In 1839, French physicist A. E Becquerel was the first to recognize photovoltaic effect. Moreover, Charles Fritts by1883 was the first to build a photovoltaic cell. He coated a thin layer of gold to the Selenium semiconductor to come up with the junction (Swanson *et al*., 2000). This device made was only about 1% efficient. The first photoelectric cell was built by a Russian Physicist Aleksandr Stoletov in 1888. It was based on the earlier photoelectric effect recognized by Heinrich Hertz in 1887 (Swanson *et al*., 2000). Patenting of the modern semiconductor junction was done by L. Pearson, Darlyl M. Chapin and Calvin S. Fuller in 1946. Much work has been done in attempt to enhance the efficiency, utilize available materials and most importantly to lower the cost of fabricating solar cells (Gall *et al*., 2009). Preview on the development of thin films from different materials (Sn, Se, Ni and SnO_2) is highlighted in this chapter.

2.2 Studies Involving Thin Film Materials for Solar Cell

A number of researchers have conducted research on diverse materials of thin films for solar applications. Among them includes $CuInSe_2$/ZnO (Kekuda *et al*., 2006) and $Cu(InGa)Se_2$ (Yin, 2014). These researches at the end of the day are meant at coming up with newer and superior solar cell materials, expanding better fabrication technologies and refining the efficiency of solar cells.

2.3 Studies Involving Nickel

Chemical element with the atomic number 28 and chemical symbol Ni is known as Nickel. At room temperature Nickel has sluggish rate of oxidation, it is considered to be resistant to corrosion. Dc Magnetron sputtering deposited Ultra-thin nickel films at room temperature

without any post-treatment. This was important for easy introduction into a common industrial process. Comparing surface analysis, electrical and characterization of Ultra-thin nickel have also been done indicating a state of a TCO. Ultra-thin nickel electrical properties was seen to be superior to those of Indium Tin Oxide (ITO) layers, while still preserving similar optical transmittance (Stefano *et al*., 2007). The surface morphology of Nickel doped Aluminium Zinc Oxide (AZO/Ni) and Aluminium Zinc Oxide (AZO) samples resolved that oxidized Ni capping layers with applicable thickness can effectively upsurge the environment stability of Aluminium Zinc Oxide (AZO) films and intensely diminish otherwise unavoidable degradation in surface morphology, electrical and optical properties (Ghosh *et al*., 2011) .

2.4 Studies Involving Pure Tin Oxide and Doped Metal Oxides

Perhaps SnO_2 is the simplest of the TCOs. Each oxygen atom of SnO_2 is surrounded by three tin atoms in a planar array and each tin is surrounded by six oxygen atoms in an octahedral array hence SnO_2 has the rutile structure. Tin Oxide is well known as an inorganic compound with a wide band gap and direct semiconductor at room temperature. These drawbacks have led to the development of Fluorine doped tin oxide (Yadav *et al*., 2008). Good optical properties on Tin based solar cells are revealed and its alloys have superior efficiency solar cell materials (Toshiyuki *et al*., 1991).

Nanoparticles of Nickel-doped tin oxide were synthesized by a method known as simple co-precipitation. Optical band gap for pure SnO_2 was revealed to be 4.06 eV and this was achieved using UV-Vis spectroscopy, then 4.08 and 4.10 eV for Ni (1 and 2 wt. %) doped SnO_2 nanoparticles, respectively (Mohsen *et al*., 2012). A simple wet chemical method has successfully synthesized nanoparticles of Ni doped SnO_2. Experimental revelation indicate that Ni is integrated into SnO_2 lattice without casting any TM cluster and/or oxide phases. The optical band gap energy of SnO_2 found to lessen with growing doping concentration, which may come about due to the formation of donor energy levels in the actual band gap of SnO_2

(Sharma *et al*., 2007). SnO_2 doped with Nickel powder samples with dopant concentrations in the range of 3 at % to 15 at % were prepared using solid-state reaction. A decrease in optical band gap was revealed with the rise of Ni doping levels (Kuppan *et al*., 2014).

Doping tin dioxide by Fe, Co, Ni, and Cu (0–16 at %) has revealed that the dopants promote both the change of the film morphology and the decrease of grain size on the conducted research during the spray pyrolysis deposition. The doping influence on both the film morphology and the grain size is weakened at higher pyrolysis temperatures 450^0C (Korotcenkov *et al*., 2008). XRD measurements has shown that the lattice volume decrease and the grain size decrease with nickel content increasing in SnO_2: Ni Nano Powders prepared by sol-gel method. An organized change in magnetic behavior from diamagnetic to ferromagnetic with increase in doping formation from x = 0.01 to x = 0.10 has been revealed in Sn_{1-x} Ni_xO_2, x = 0.01 to x = 0.10 nano powders created at 450°C (Vadivel *et al*., 2011).

2.5 Studies Involving Tin Selenide Thin Film

Metal chalcogenides have attracted attention of many researchers. This is because, comparing to other researchers they have shown good performance (Lindgren *et al*., 2002). Various researchers have used metal chalcogenides to synthesize thin films.

A number of researchers have attracted the attention of Tin selenide owing to their fascinating optical and electronic properties (Gullen *et al*., 2011). Tin selenide is thus used in fabricating solar cells because it is best in absorbing enormous share of solar energy. This material is also vital for various optoelectronic applications like light emitting devices, light emitting devices, holographic recording systems, memory switching devices and many others (Kumar *et al*., 2012). Tin selenide has a narrow band gap of about 1.1 eV and therefore a superior p-type semiconductor (Kumar *et al*., 2012). X-ray diffraction reveals that Tin selenide crystallizes

with an orthorhombic structure consisting of irregular packed atoms with two-fold harmonized selenium atoms mixed with two-fold harmonized tin atoms (Chung *et al.,* 2008).

Taut bound two layers existing in selenium and tin atoms suggests that the bonding between the layers form weak van der Waals type stacked end to end to the crystallographic c-axis of SnSe composition, which leads to a highly articulated layered type of composition. This composition and arrangement of SnSe makes it attractive for the fabricating of solar cells, because of higher chemical stability with no passiveness in comparison to other semiconductors, for example GaAs, CdSe and Si which require exceptional passiveness procedures in order to avoid photo corrosion (Aruchamy, 1992). Various deposition techniques for SnSe thin films preparation have been used. Chemical precipitation technique (Zainal *et al*., 2013), chemical vapor deposition (Zhiyong *et al*., 2002), thermal evaporation (Kumar *et al*., 2011), spray pyrolysis (Mariappan *et al*., 2010), Pulse Laser deposition method (Zheng *et al*., 2011) among others. Among them spray pyrolysis is the utmost and commonly engaged method since it is very economical, convenient and simple technique mainly used in the large-area devices fabrication (Mariappan *et al*., 2010).

$SnSe_2$ and its composite film SnSe was prepared by controlling heating conditions and thickness of films. The optical band gap of 1-1.27ev and conductivity of 0.02-0.2 $(\Omega cm)^{-1}$ were obtained (Bindu and Nair, 2004). Substrate temperature ranging from 400°C to 500°C of SnSe thin films were obtained. Acceptable values of resistivity and mobility were obtained at a temperature of 450°C. $SnSe_2$ thin films were obtained in the substrate temperature range from 270°C to 300°C. At 270°C $SnSe_2$ forms acceptable values of resistivity and mobility. The result obtained indicates the possibility to use these materials in a photovoltaic structure built completely by Ultra sonic Spray Pyrolysis technique (Jorge *et al*., 2015). Chemical bath deposition technique has been used to prepare thin films of SnSe. It was revealed that reflectance of films was low in entire region of the electromagnetic spectrum. This make the

films good glazing material in warm climatic regions for solar control (Okereke *et al*., 2012). The results of Zn:Se ratios on the photo conducting and absorption properties were analyzed after spraying ZnSe thin films. It was noted that the reduction in band gap energy with the increased Se ratio in the thin film can be associated to the increase in the grain size of the thin film (Oztas *et al*., 2004).

SnSe and $SnSe_2$ thin films were deposited by the spray pyrolysis. Thin films of $SnSe_2$ were coated using a solution flow rate of 5 ml/min at substrate temperatures in the range of 325 °C to 375 °C and good optoelectronic properties were reported. The optical band gap of the films were obtained as 1.59 eV. The conductivity of the material which is n-type is of the order of 10^1 $(\Omega\ cm)^{-1}$. When the flow rate was raised to 8 ml/min, a mixture of the $SnSe_2$ and SnSe compounds was obtained at the deposition temperature ranging from 275 °C to 325 °C. When the samples are annealed at a temperature of 250 °C in 5% hydrogen and 95% nitrogen environment for 2 h, the SnSe – $SnSe_2$ thin films led to crystallization of SnSe compound. Annealed thin films analyzed optically reveals that the films are p-type having a direct allowed band gap of 0.81 eV and a conductivity of around $2\times10^1\ \Omega\ cm^{-1}$ (Martínez-Escober *et al*., 2013). Thin film of SnSe showing polycrystalline structure was coated by vacuum deposition at a substrate temperature of 150^0C. Photosensitivity increased with illumination on the thin film of SnSe (Pathinettam *et al.,* 2000). A study on effect of substrate temperature on growth of SnSe thin film deposited by evaporation method was done. It was noted that the electrical resistivity varied from 3.0-8.1 Ωcm^{-1} with the variation of thickness in the range of 150-300 nm (Hema *et al*., 2007). Characterization of SeSn (n-SnSe) thin film was synthesized by thermal evaporation technique in the presence of argon carrier gas. The value of band gap was obtained as 2.18 $\pm$0.01 eV which was an increment in comparison to the bulk value of 1.68 $\pm$0.01 eV (Sharma *et al*., 2007).

Deposition of thin films of Sn_xSe_y and ZnO:Al was done by thermal evaporation and reactive thermal evaporation techniques respectively. The study found that the fabricated solar cell, SnSe-ZnO:Al/Ag, had a short circuit current of 1.06mA/cm^2, open circuit voltage of 0.59V, fill factor of 0.65 and an efficiency of 0.41% (Charles *et al*., 2011). In SnSe-CdO:Sn P N-junction fabrication, highest transmittance, low absorption and low reflectance are some of the factors which were considered when choosing the window layer for PV applications while high absorption coefficient and low reflectance are needed for an absorber layer. The diode characteristics obtained were; Isc = 0.993 mA, I_{max} = 0.905mA, Voc = 273mV, V_{max} = 207mV, FF = 0.69, and an efficiency of 0.59% (Nyakundi, M.E. 2014).

CHAPTER 3

THEORETICAL BACKGROUND

3.1 Solar energy and Solar cell

Light and radiant heat from the sun that stimulate earth's weather, climate, and sustains life is the Solar energy. It is one of the abundant renewable energy which is non-polluting in our planet. The geographical locations determines how much solar energy is received. If the total desert land of 50×10^7 Km^2 receives solar radiation for 8 hours a day, then the solar received is 1.632×10^{14} Kwh/year (Waita, 2008). If each solar panel is 1% efficient, this would translate to 1.632×10^{12} Kwh/year. The above figures exceeds the world's energy need. If only ten minutes is utilized per day then it would be enough to provide the worlds annual needs (Markvart and Castaner, 2005). Solar cells can also be concentrated using flat collectors or solar concentrators.

A device that convert solar energy into electrical energy is known as a Solar cell. For it to generate maximum electrical power when subjected to sunlight this p-n junction diode is optimized (Sanjay *et al*., 2009). Once light energy is directed on to the cell an electron in the valence band absorbs it thereby exciting it to the excited electronic states leaving a hole in the valence band. Free charge carriers which are holes and electrons give rise to the photo current. Both hole and electron can move haphazardly in the privation of electric field and occasionally can recombine (Sanjay *et al*., 2009).

3.2 p-n Junctions.

Holes diffuse from the p-type semiconductor into the n-type when free electrons diffuse from the n-type into the p-type in a p-n junction (Singh, 2003). The mobility of these charge carriers comprises the diffusion current. Diffusion of electrons from the n-type towards the p-type semiconductor, make a region on n-type semiconductor remain with positively charged atoms.

In the same way, as holes diffuse into the n-type semiconductor from the p-type semiconductor, makes the p-type matter remain being negatively charged. This process causes a creation of a region known as depletion region displayed in the figure 3.1 (b). Figure 3.1 (a) shows a schematic diagram of discrete n-type and p-type materials and figure 3.1 (b) shows the p-n junction made.

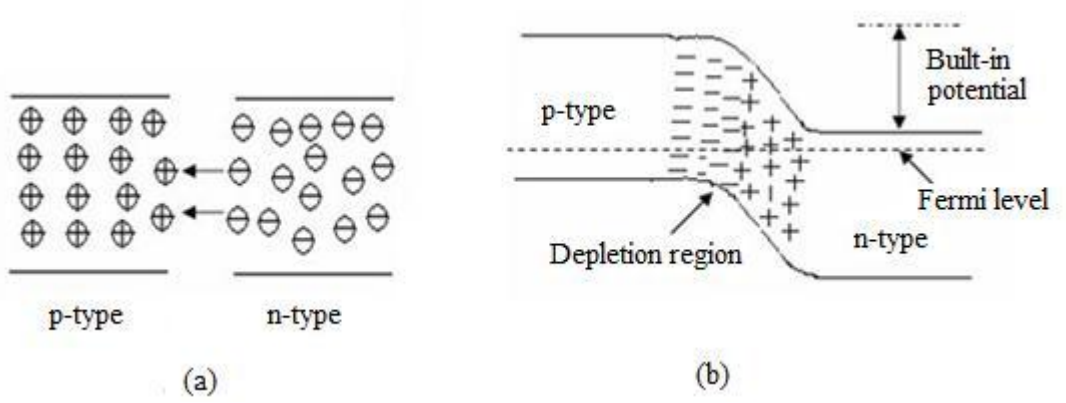

Figure 3.1: P-type and n-type schematic diagram (a) Before amalgamating and (b) After amalgamating p-type and n-type materials.

Static charges are formed on both the n-type and p-type matter close to the junction as electrons and holes diffusion go ahead (Gowri, 2003). Electric field is set up around the charged area which bring about a second generation current called the drift current. The diffusion current moves in the opposite direction of the flow of drift current. In the beginning, drift current is over-powered by the diffusion current, but as diffusion proceeds, the potential influencing the drift current is enhanced resulting to higher drift currents and when the diffusion balance with the drift current, they actually match. Ionized acceptors and donors builds up an electric field at the junction expressed as:

$$E = -\Delta . V \qquad (3.1)$$

the electric field for one facet is expressed as:

$$E = -\frac{dV}{dx} \tag{3.2}$$

The junction is brought into equilibrium when the diffusion process is restricted by the electric field. Current densities at equilibrium circumstances are expressed as:

$$J_{diffusion} + J_{drift} = 0 \tag{3.3}$$

Holes and electrons jointly accounted for in the p-n junction (Sze, 1991), the total current is expressed as:

$$I = I_o \left[\exp\left(\frac{qV}{kT}\right) - 1\right] \tag{3.4}$$

where I_o is the reverse bias saturation current, V is voltage across the junction, I is current through the junction, q is the electron charge, T is the absolute temperature and k is the Boltzmann constant.

Between two semiconductors interacting, there are several types of junctions (Brennan, 1996). In case the n-type and p-type regions materials are similar, the junction is known as homojunction, but if it happens that the p-type and n-type are not the same, the junction is known as heterojunction. Heterojunction is mainly used in fabricating solar cells with absorber layer having a narrow band gap and window layer having a wide band gap in order to reduce the surface recombination losses that in other ways take control in direct band gap materials. A p-n junction which works on the photovoltaic effect principle and on its either sides has electrical contacts is called a solar cell.

3.3 Heterojunction

An interface created between a wide band gap n-type semiconductor and a p-type semiconductor with a narrow band gap is known as a heterojunction.

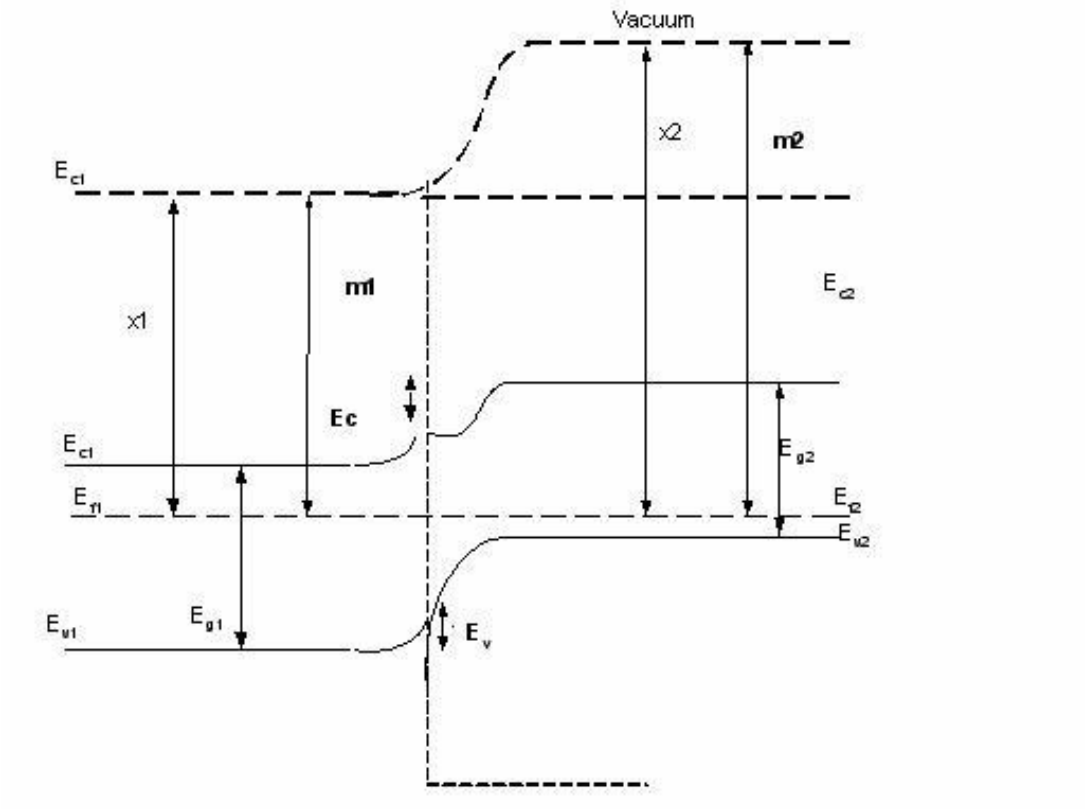

Figure 3.2: Heterojunction at equilibrium Energy band diagram (Gowri, 2003).

In the diagram (figure 3.2), the electron affinities are shown by x1 and x2, work functions are Φm1 and Φm2 and E_{g1} and E_{g2} are band gaps of two different materials.

Valence band induced and discontinuities in the conduction are represented by $Ev = E_{g1} - E_{g2} - \Delta E_c$ and $Ec = (x1 - x2)$ as shown above in figure 3.2 due to the different work functions, the band gaps and electron affinities of the materials. An absorber layer is formed by a narrow band gap material whereas a window layer is made by a wide band gap material in applications of solar cells (Gowri, 2003). Photon energy incident on the absorber layer is absorbed and an electron is injected from the valence band to conduction band when the energy is greater than the band gap energy and electron hole pairs are created.

3.4 Charge Carrier kinesis in semiconductors

At room temperature, electrons in a semiconductor flows haphazardly under the thermal

equilibrium. Individual electron thermal velocity (thermal motion) may be seen as a series of irregular collisions with other scattering centres, lattice atoms and impurity atoms (Serhan, 2005). The moment a semiconductor is applied with a an electric field, each electron will be accelerated along the field due to the force it experiences from the field and flows in the opposite direction from the field. These electrons under the influence of the field acquires a velocity known as a drift velocity. The connection between the electric field applied to the semiconductor and electrons drift velocity is given by the equation:

$$V_n = -\mu_n E \qquad (3.5)$$

where E is the electric field; Vn is the drift velocity of electrons and μ_n is the electron mobility given by the relation:

$$\mu_n = \frac{q\tau_c}{m_n} \qquad (3.6)$$

where $m_n$the effective mass, τ_c is the mean free time that is the average time between collisions. Because of the fact that effective mass of an electron is smaller than that of a hole, the electron Kinesis is greater than that of a hole.

Similarly, the hole's drift velocity is given by the relation:

$$V_p = -\mu_p E \qquad (3.7)$$

Where E is the electric field, V_p is the drift velocity of the holes and μ_p is the hole mobility.

An applied electric field influences the transport carrier producing a drift current. The current density of an electron is given by the relation:

$$J_n = -qnV_n \qquad (3.8)$$

Which in terms of E this can be rewritten as:

$$J_n = qn\mu_n E \tag{3.9}$$

current density of the holes is related by:

$$J_p = qpV_p \tag{3.10}$$

Whose modification can be given as:

$$J_p = qp\mu_p E \tag{3.11}$$

where *n* is the concentration of electrons and *p* is the concentration of holes per unit volume and *q* is the electronic charge, respectively.

Hence, the semiconductor sample total current density is given by relation:

$$J = J_n + J_p \tag{3.12}$$

Using equations (3.9) and (3.11) equation (3.12) can be rewritten as:

$$J = \left(qn\mu_n + qp\mu_p\right)E \tag{3.13}$$

This can be reduced to:

$$J = \sigma E \tag{3.14}$$

where the conductivity of the semiconductor is given as $\sigma = qn\mu_n + qp\mu_p$ which is determined by the concentration of the charge carriers *p* and *n*. The temperature in an exponential way determines the number of charge carriers, and with increasing temperature increases very rapidly. Therefore, temperature increase leads to the conductivity also increasing in a similar fashion.

The resistivity of the semiconductor is given by the relation:

$$\rho = \frac{1}{\sigma} \qquad (3.15)$$

The characterization thin doped films is done using sheet resistance idea, since it is relatively easier to determine the sheet resistance instead of the resistivity of the material. The uniformly-doped film sheet resistance of a given thickness, *t*, and resistivity, ρ and is given by relation:

$$R_s = \frac{\rho}{t} \qquad (3.16)$$

3.5 Thin film Solar cells

Solar cells made of thin films are mainly fabricated by physical or chemical methods. Because of thin film technology being produced at a lower cost and a likelihood for mass production, it has attracted much of commercial attention (Zhou, 2008). Lessening the cost of thin film method is achieved by using inexpensive processing and less amount of material. The thickness of thin film is in the range of a fraction of nanometer to more than a few micrometres. Molecule to molecule or atom to atom condensation process is what form a thin film. Depending upon the field of application the limit of thickness may range from a nanometer to a handful micrometer (Chopra & Krieger, 1969). By means of lowering the cost of photovoltaic structures substantially development of thin film technologies takes place.

Generation of current involves two processes in thin film solar cell, these includes: photons energy absorption and generation and collection of electron hole pairs. Once the charge carriers are generated, the holes and the electrons are separated and then collected at the contacts. Charge carrier separation takes place in two main modes: diffusion of carriers from a region of high carrier concentration to lower carrier concentration through potential gradient of an electrochemical in a p n junction and drift of carriers, due to build in electrostatic field. The moment photon energy is absorbed whose energy is more than the band gap energy, generation of current takes place by a process called photovoltaic effect.

Creation of voltage or current in photovoltaic devices is photovoltaic effect which is as a result

of shining of light on the device. The photocurrent generated is the electron hole pair. These electron hole pairs are mobile carriers and in this case called photo carriers and they are more than equilibrium concentration. In a p n junction, excess charge carriers either recombine or get collected. Annihilation of a hole electron pair is known as recombination whereas when an electric field separate electrons and holes causing a photocurrent is referred to as collection (Gowri, 2003). PV operations is thus centred on three features; the photon energy absoption which generates either excitons or electron-hole pairs, separation of electron hole pairs and the movement of electron holes to the external circuit. The energy band gap diagram showing the absorption of photon and creation of electron hole pair of a solar cell is shown in the figure 3.3

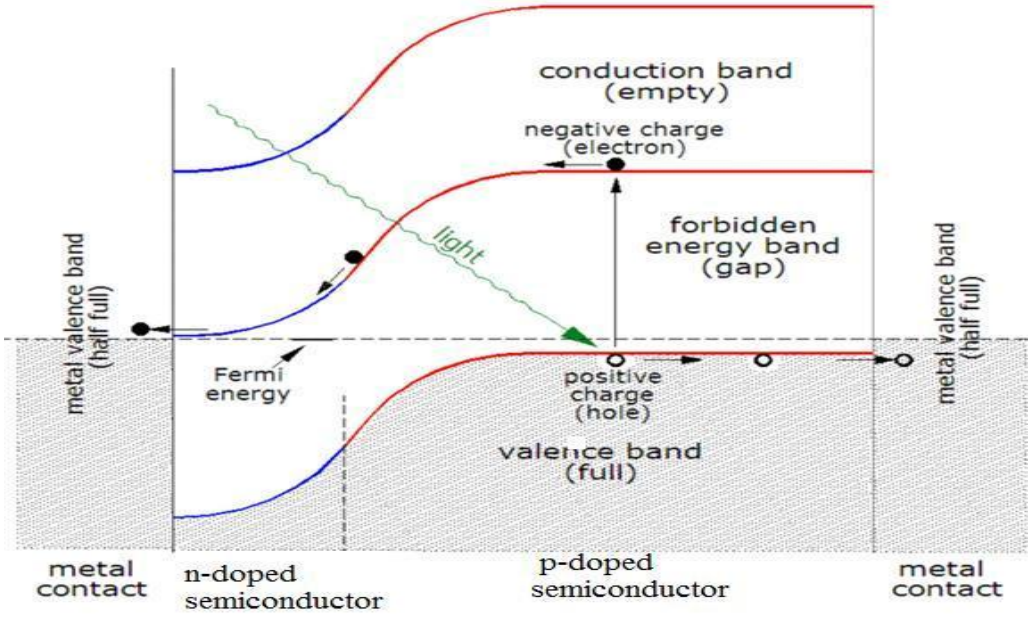

Figure 3.3: Energy band schematic diagram of a solar cell under shining of light.

Between the window layer and absorber layer of a thin film solar cell, there exist a junction. Photon energy pass through the window layer towards the absorber layer and electron hole pairs are generated and flows through the external load in form of current as shown in figure 3.4. No generation of photocurrent that takes place in the window layer.

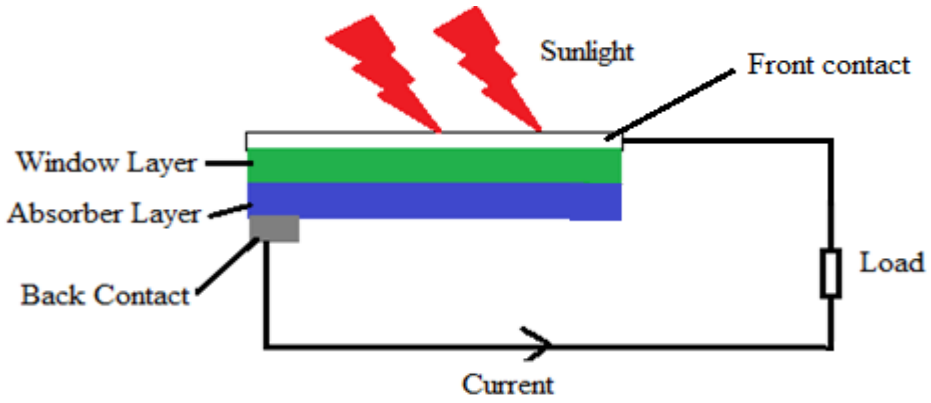

Figure 3.4: A solar cell Schematic diagram connected to an external load.

3.6 Performance and Parameters of a Solar cell

The current-voltage of illuminated PV solar cell is given by the following relationship,

$$I = I_o \left[\exp\left(\frac{qV}{AkT}\right) - 1\right] - I_L \qquad (3.17)$$

where V is voltage across the diode, I is current through the diode, I_L is the light generated current, I_o is the reverse bias saturation current, T the absolute temperature, k is the Boltzmann constant (8.62×10^{-23}eV/K) and q is the electron charge.

When infinite load attached, to obtain voltage, the same relationship is expressed as;

$$V = \frac{kT}{q} \ln\left[\frac{I}{I_o} + 1\right] \qquad (3.18)$$

The I-V characteristics of a solar cell under illumination and dark conditions is shown in the figure 3.5

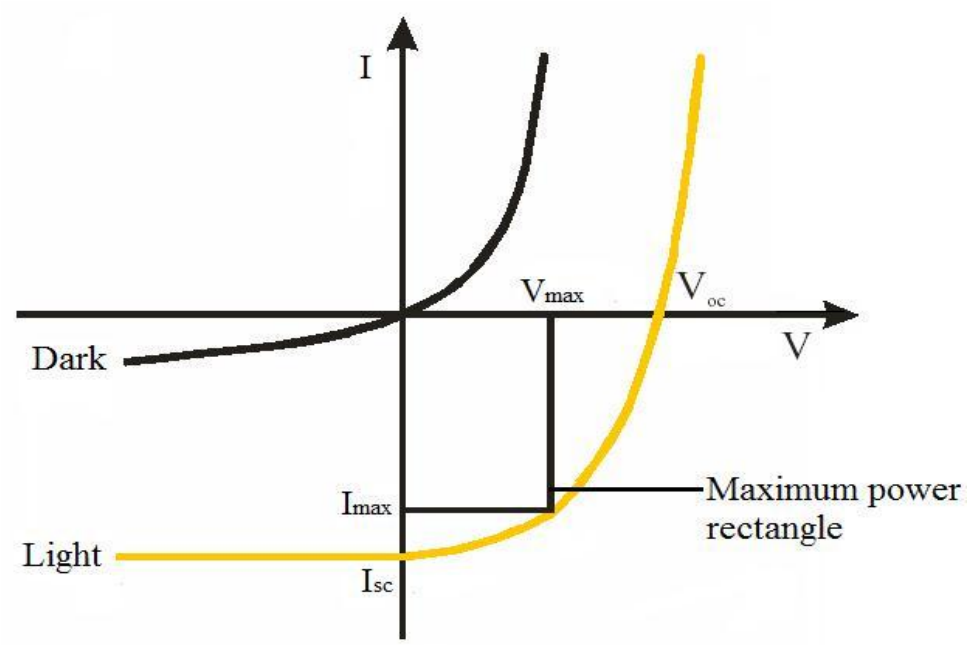

Figure 3.5: The I-V characteristics of a solar cell under illumination and dark conditions (Sumbit, 2008).

A solar cell is merely a diode, in the dark. When photons are incident on a semiconducting material and whose energy is greater than the band gap energy, there is excitation of electrons. Hence, generated current flow in the solar cell.

3.6.1 Open-circuit voltage (V_{oc}) and Short-circuit current (I_{sc})

Under short circuit conditions, current is obtained which is known as short circuit current, I_{sc}. This is the current when voltage is zero. In dark, no current flows in the circuit and solar cell (short circuit) are connected through a conductor. The tendency of charge carriers flow by the impending effect of the potential barrier at the junction and by diffusion brings about a delicate balance. When light illuminates on the diode, the balance is tipped and short circuit, I_{sc}, moves through the circuit. Therefore, from the Shockley ideal diode equation the short-circuit current, I_{sc}, is given using equation;

$$I_{sc} = -I,\ V = 0 \qquad (3.19)$$

At the point of intersection along the voltage axis of the curve, we obtain the open circuit voltage, V_{oc}, under illumination, which is the output voltage across the terminals of the device when infinite load is attached on it (zero current). Some voltage, V_{oc}, is necessary to bias the structure under open circuit conditions to counter the induced current. Built in electric field present in the materials system brings about open circuit voltage, V_{oc}, and short circuit current, I_{sc}. The equation of Shockley ideal diode is again used to give open-circuit voltage, V_{oc}, expressed as;

$$V_{oc} = V, \text{ and } I = 0 \qquad (3.20)$$

Therefore, the output voltage with infinite load attached to the device terminals (I = 0) is known as the open-circuit voltage, V_{oc}.

As shown in figure 3.5, V_{max}, is maximum voltage at the maximum power output, P_{max}, whereas I_{max}, is Maximum current at the maximum power output, P_{max}, of the solar cell

3.6.2 Fill Factor (FF) and efficiency (η) of a solar cell

The current-voltage curve of a solar cell measurement of the squareness is known as fill factor, FF. Fill factor, FF by definition is current multiplied by voltage at the maximum power point over the open-circuit voltage multiplied by short-circuit current, i.e.,

$$FF = \frac{V_{max} I_{max}}{V_{oc} I_{sc}} \qquad (3.21)$$

Therefore, the difference from an ideal cell to how far the Current-Voltage characteristics of an actual solar cell gives a measure of fill factor, FF.

The efficiency, η, of a solar cell is defined as the ratio of the maximum power output, P_{max}, of the solar cell to the incident power on the cell. It is the extent of conversion of light (photon) energy into electrical energy. This equation is given by the expression below;

$$\eta = \frac{P_{max}}{E \times A} \times 100 \qquad (3.22)$$

When the area of the rectangle is maximum we obtain maximum power, P_{max}. The efficiency, η, can also be given in terms of the Fill Factor considering equation 3.22, as;

$$\eta = \frac{V_{oc} I_{sc} FF}{P_{in}} \times 100 \qquad (3.23)$$

where P_{in}, is the incident solar power illuminated on the solar cell usually given in W/m^2 and $P_{max} = V_{max}\ I_{max}$.

3.6.3 Equivalent circuit of a solar cell

Zero series resistance (R_s) and infinite shunt resistance (R_{sh}) should be found in an ideal solar cell. In a practical solar cell Rs and R_{sh} are existence unlike in an ideal solar cell. The leakage currents in the bulk or across the perimeter can bring about low shunt resistance. Lower V_{oc} and poor fill factors comes as a result of low shunt resistance. The leakage current is low and insignificant in single crystals. Grain boundaries in thin films causes high leakage currents which is brought about by shunting paths. The contact resistance and the bulk resistivity mostly affect series resistance (Rs). Figure 3.6 shows equivalent circuit of a solar cell.

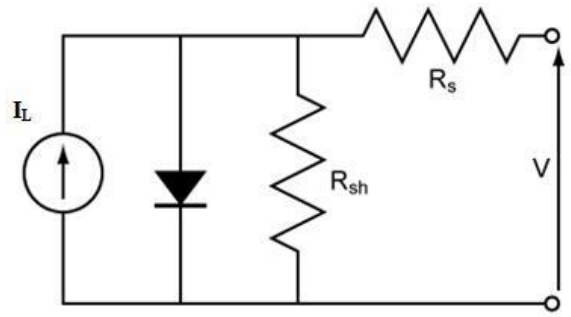

Figure 3.6: Schematic diagram of an equivalent circuit of solar cell

3.7 Characterization of thin film

3.7.1 Optical properties and measurements

When light is illuminated on a semiconductor, intensity of transmission, absorption and reflection can be measured. A lot of information such as band gap of the material can be obtained pertaining a semiconductor from these optical effects (Ranjdar *et al.*, 2006). Photons of high energy are absorbed by electrons from the filled valence band state which switch to the empty conduction band state. Radiation is absorbed for the energies reasonably below the lowest forbidden energy band gap owing to the electron transitions between band and impurity states and the formation of excitants. As photon energy decreases, absorption continuum which is produced by the transitions of free charge carriers within the energy bands increases. Similarly, radiation absorption can take place within the crystalline lattice itself, with the optical phonons giving off energy. Lastly, at long wavelengths or at low energies, between impurities and their associated bands, observation can be made on electron transitions. Vital technological applications are noted upon many of these processes; for instance, band to band absorption is utilized by the intrinsic photo detectors. However, laser semiconductors commonly function by way of transitions between band states and impurity.

3.7.2 Optical absorption

In determination of band gap energy, incident photons optical absorption is vital. Comparatively, transmission of photons is observed when a particular wavelength is incident to the sample. Considering that the photons with energies lower than the band gap are transmitted whereas the photons with energies greater than the band gap are absorbed ie ($h\nu \geq$ Eg). The absorbed or transmitted photon measurement can give the band gap energy of the thin film (Sumbit, 2008). The α which is the absorption coefficient per unit length is expressed as:

$$\alpha = \frac{4\pi k}{\lambda} \qquad (3.24)$$

where, *k* is the absorption constant and λ is the wave length of illuminated photon of the sample.

Complex dielectric constants characterizes an absorbing sample which is given by the equation,

$$\varepsilon = \varepsilon_1 - i\varepsilon_2 \qquad (3.25)$$

The dielectric constants real and imaginary parts of the of the films ε_1 and ε_2 respectively can be established from the equations,

$$\varepsilon_1 = n^2 - k^2 \qquad (3.26)$$

And

$$\varepsilon_2 = 2nk = \frac{4\pi\sigma}{\omega} \qquad (3.27)$$

where, σ is the dc electrical static conductivity and ω is the incident light angular frequency.

The ability of a material to be polarized by the influence of electric field gives a measure of its permittivity. Which is dependent on frequency.

Optical radiation is absorbed by engendering excitation from one level to a higher level in semiconductors on condition that energy of radiation hυ is same to or more than the distinct in energy between the two participating levels. Transmittance through the film of thickness (d) and the intensity of radiation *I* dependence is of the form:

$$\mathrm{I} = \mathrm{I_o}\exp(-\alpha \mathrm{d}) \qquad (3.28)$$

where α is the absorption coefficient and I_0 is the initial intensity of radiation (Pankove, 1971).

The optical constants such as complex refractive index($n^* = n - ik$), refractive index, *n*, and absorption coefficient (α), extinction coefficient, *k*, and dielectric constant ε of the semiconductor are determined with the help of the optical, absorption, reflection and transmission properties of a material. Vital physical properties of the film relates real part of refractive index (*n*) for instance the reflectance spectrum, which consecutively is related with

the band structure (Born *et al.*, 1975).

3.7.3 Transmittance and reflectance

Reflectance and transmission of a structure rest on optical constants, extinction coefficient *k*, the film thickness *d*, of the film, refractive index n of the film, the index of refraction n_s of the substrate, the wavelength λ, of light. The reflection coefficient R and transmission coefficient T are the two vital quantities mostly measured and for normal incidence they are expressed as:

$$T = \frac{(1-R^2)\exp(-4\pi x/\lambda)}{1-R^2\exp(-8\pi x/\lambda)} \tag{3.29}$$

$$T = \frac{(1-n)^2+k^2}{(1+n)^2+k^2} \tag{3.30}$$

where, *x*, is the thickness of the sample, λ, is the wave length of radiation, *k*, extinction coefficient and *n*, the refractive index of the film.

3.7.4 Refractive index and extinction coefficient

The reflectance R, and transmission T, of the system vary with optical constants, the thickness, *d*, of the film, refractive index *n*, extinction coefficient *k*, and the substrate of the index of refraction, n_s and the wavelength of light, λ (Brennan, 1999).

The values of extinction coefficient *k*, film thickness *d*, and refractive index *n*, can be obtained by constructing enclose functions T_{max} and T_{min} from transmission measurements treated as continuous functions of wavelength λ. However:

$$n\left[N + (N^2 - n_s^2)^{\frac{1}{2}}\right]^{\frac{1}{2}} \tag{3.31}$$

With $$N = \frac{(1+n_s^2)T_{max}T_{min}}{2+2n_s(T_{max}-T_{min})} \tag{3.32}$$

The two maxima or two minima can be used to calculate the thickness *d*, of the film using the

expression:

$$d = \frac{M\lambda_1\lambda_2}{2[n(\lambda_1)\lambda_2 - n(\lambda_2)]\lambda_2} \quad (3.33)$$

where two extremes afoot at λ_1 and λ_2, gives the number of oscillations M.

3.7.5 Energy band gap

Basic optical absorption edge is achieved by means of the energy band gap in a semiconductor. Photon energy is absorbed and excitation of an electron takes place during this basic absorption process from a filled valence band state to an empty conduction band state. It is impossible for such process to take place when the photon energy is less than the band gap energy since it is not absorbed. Therefore, transmission of the electromagnetic radiation takes place in the semiconductor (Ranjdar *et al.*, 2006).

Optical absorbance against wavelength gives the data which facilitates derivation of the transmission types and band gap energy by mathematical relationship shown below about the absorption edge.

$$\alpha = \frac{(h\upsilon - E_g)^{\frac{n}{2}}}{h\upsilon} \quad (3.34)$$

where h is the Planck's constant, υ is the frequency, whereas n takes the value of probable 1 or 4. n gives the transition kind whichever can be direct transition or indirect transition between the semiconductor states. For instance when n = 1, $(\alpha h\upsilon)^2$ against the photon energy ($h\upsilon$) is plotted, and the linear graph which cuts the photon energy ($h\upsilon$) axis gives the direct band gap value (Zainal *et al.*, 2003). Figure 3.7 shows E-k diagrams representing the direct and indirect electron absorption. Optical modes and photon's dispersion relation intersection takes place awfully close to k = 0 in optical phonon modes. This is since in the crystal lattice, the photon wavelength λ is much elongated than a typical inter-atomic spacing, a, at the relevant

frequency. Therefore, $K_{photon} = \frac{2\pi}{\lambda}$ photon is too small on the scale of the Brillouin zone $k_{BZ} = \frac{\pi}{a}$. On the band diagram interband electronic transition is fundamentally vertical. $Hk_{photon} = hk_{electron}$ is needed to conserve momentum and this condition is satisfied if the minimum of the conduction band (CB) and the maximum of the valence band (VB) happen at the constant k-value; habitually at k = 0. Figure 3.7(a) shows a direct energy gap. If the CB minimum and VB maximum occurs at different k-value, as shown in figure 3.7 (b) the gap is aforesaid to be indirect energy gap

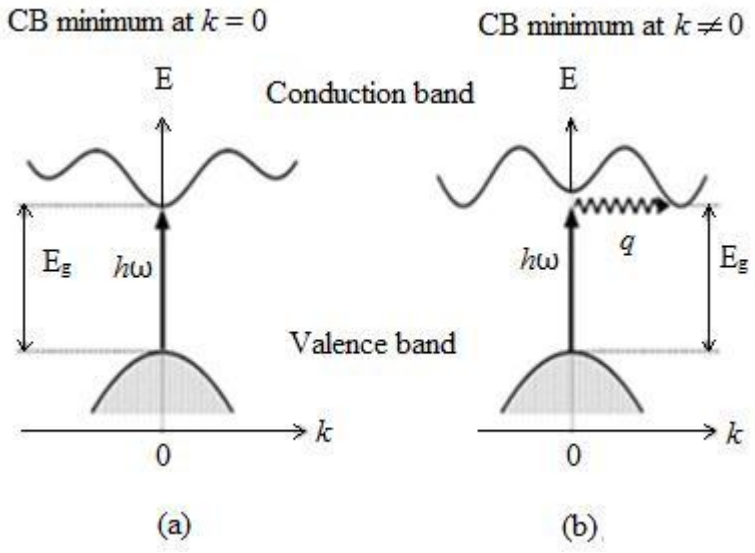

Figure 3.7: (a) Transition of direct band gap (b) Transition of indirect band gap (Ranjdar, 2006).

3.8 The SCOUT software

Scout software is a 32 bit software for windows 98/NT/2000/XP/Vista software. It is used for the analysis and simulations of optical spectra such as absorbance, Attenuated total reflection (ATR), reflectance, transmittance, ellipsomery, and electroluminescence (Theiss, 2001). It is also used to verify thin film compositions and thickness. The spectral can range, from mid and far infrared, Visible, NIR or UV regions. The data simulation by this software is done using various models. Three SCOUT models are used pertaining this work.

3.8.1 The Drude model

German Physist, Paul Drude 1863-1906 came up with this model and the model named after him. Electrical and optical properties of a material are linked with the performance of its holes or electrons by this model. Mostly in metals, it explicate the flow dynamics of electrons and other materials. Kinetic theory applies for this model which presume that the electron microscopic performance in solids may appear similar to a pin ball when treated classically with a pool of re-bouncing of barely heavier immobile positive ions and constantly jittery bouncing electrons.

Once "free electrons" are isolated, a number of positively charged ions remain. These happened when the valence levels of the atom came in interaction with atoms potential. Drude model assume any extended range contact between ions and electron notwithstanding the origin of free electrons from the interaction of dissimilar potential and presume that the electrons do not interrupt each other. Instantaneous collision between an ion and a free electron is the only probable interaction which occur with an immovable likelihood per unit time. Both ions and electrons are treated as solid spheres by the Drude model which is purely a classical model.

Hence, this model provides a good explanation of the Hall effect, AC and DC conductivity in metals and thermal conductivity (due to electrons) at room temperature in metals.

3.8.2 The O' Leary-Johnson-Lim (OJL) model

The OJL is used in amorphous materials to illustrate the inter band transition (O"Learly *et al*., 1997). The density of states for the optical transition expressions is given by OJL inter band model from the valence band to conduction band. Parabolic bands are assumed with tail states exponentially decaying into the band gap. The OJL density of states model original parameters are energy E_c and E_v and the conduction and valence bands "damping constants", γ_c and γ_v respectively. Similarly, the masses of the conduction and valence bands, m_v and m_c are

included. The equations given as

$$E_{M,C} = E_C + \frac{1}{2}\gamma_C \quad (3.35)$$

and

$$E_{M,V} = E_V - \frac{1}{2}\gamma_V \quad (3.36)$$

Refer to the conduction and valence bands mobility edges respectively.

E_o, the mobility gap, in the OJL is hence expressed as:

$$E_C = \frac{1}{2}\gamma_C - \left[E_V - \frac{1}{2}\gamma_V\right] = E_o \quad (3.37)$$

The difference between E_V and Ec values is the band energy, E_g, i.e. the band gap in the circumstance of no disarrangement, which is achieved when both E_C and Ev are zero. This mobility band gap is different from this gap energy which be contingent on the values of the disarranged parameters E_C and Ev. The simulation of optical band energy was done by SCOUT 98 software (Theiss, 2001).

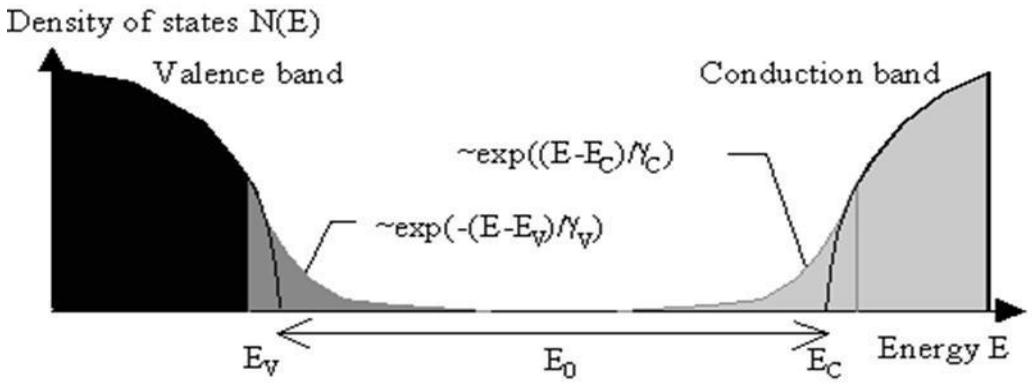

Figure 3.8: A semiconductor density of states versus the energy graph (Theiss, 2001)

3.8.3 Harmonic oscillator

A system that moves to and fro about the equilibrium position is referred to as Harmonic oscillator. This case concerns atomic nuclei motion (which are a lot weighty than the electrons) and in the infrared region usually have their resonance frequencies. These frequencies characteristic are determined by the masses moving to and fro and can be used for identification of the material because of their strength of the bonding between them, as applied for IR spectroscopy in analytical chemistry. Similarly in the case of silicon, vital impurities such as oxygen and carbon are detected by their vibrational modes characteristic.

3.9 Electrical characterization

3.9.1 Four-Point Probe method

Sheet resistance of a semiconductor material was measured by an instrument known as four point probe method. Four point probe can measure either thin film or bulk samples. The samples whose sheet resistance is to be measured should have a very small contacts on which the probes are attached i.e materials used to make the probes and point contacts should be the same. Lateral dimensions of the film must be comparable to the thickness of the film which should be very small. The probes are supposed to be equally spaced when using four point probe method. Impedance contribution of contact resistance and the wiring is eliminated by the separation of voltage and current electrodes which is the main advantage of four point probe method.

3.9.2 Thin film sample sheet resistance (R_s)

Figure 3.9 shows a square geometry thin film taken into consideration, for a very thin film (probe spacing, s >> thickness, t), current rings rather than current spheres are obtained (Brown & Jakeman, 1996).

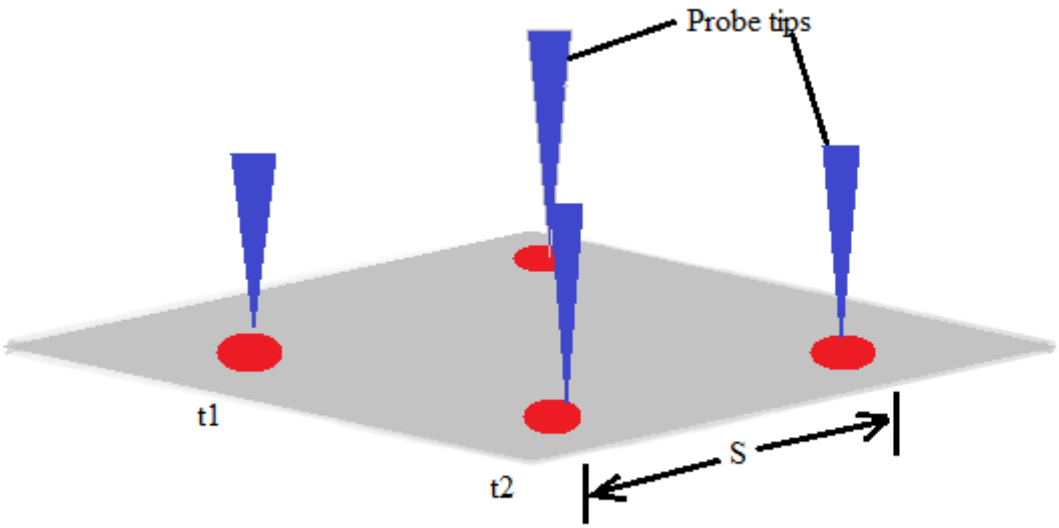

Figure 3.9: Probe tips square geometry on film sample surface (Brown &Jake man, 1996).

The area of the current ring is therefore,

$$A = 2\pi xt \tag{3.38}$$

where t, is the film thickness and x the radius of the ring

whereas sheet resistance Rs is given by equation (3.39)

$$R_s = \int_{x_1}^{x_2} \rho \frac{dx}{2\pi xt} \tag{3.39}$$

$$= \int_{s}^{2s} \frac{\rho}{2\pi t} \frac{dx}{x} \tag{3.40}$$

where s, is the probe spacing and ρ is the resistivity

$$= \left[\frac{\rho}{2\pi t} lnx\right]_{s}^{2s} \tag{3.41}$$

$$= \frac{\rho}{2\pi t} ln2 \tag{3.42}$$

Considering $R = \frac{V}{2I}$, the thin film sheet resistivity is expressed as;

$$\rho_s = \frac{\pi t}{ln2}\left(\frac{V}{I}\right) \tag{3.43}$$

It is the seen that equation 3.43 is not dependent on the s, probe spacing. Further, this equation is on many occasions used semiconductor film for characterization. Generally, sheet resistivity

can be expressed as

$$\rho_s = Kt\left(\frac{V}{I}\right) \tag{3.44}$$

where k, is a geometric factor. k = 4.532, in the circumstance of semi-infinite thin film, which from the derivation it is just $\frac{\pi}{ln2}$ and for non-ideal sample, it will be different. Therefore sheet resistance and resistivity can simply be expressed as;

$$R_s = 4.532\left(\frac{V}{I}\right) \tag{3.45}$$

$$\rho_s = 4 \cdot 532t\left(\frac{V}{I}\right) \tag{3.46}$$

3.10 Spray Pyrolysis technique

One of the technique which can be used to prepare films of porous oxides and ceramics coatings and powders is a spray pyrolysis. Other than other techniques of film deposition, spray pyrolysis was chosen because it can allow large substrates deposition, it can accept easy doping, it is also easy to set up, it has minimal waste during production and comparatively a method which is cost effective particularly as pertaining the cost of equipment. The films made have properties that are reproducible therefore the technique is suitable for bulk production. A substrate heater and its controller, precursor solution and an atomizer are what constitutes a spray pyrolysis. Figure 3.10 shows a spray pyrolysis set up. A thermal couple is used to record the desired substrate temperature. A gas from the cylinder at a set pressure sprays the precursor solution through the nozzle which is deposited on the substrate.

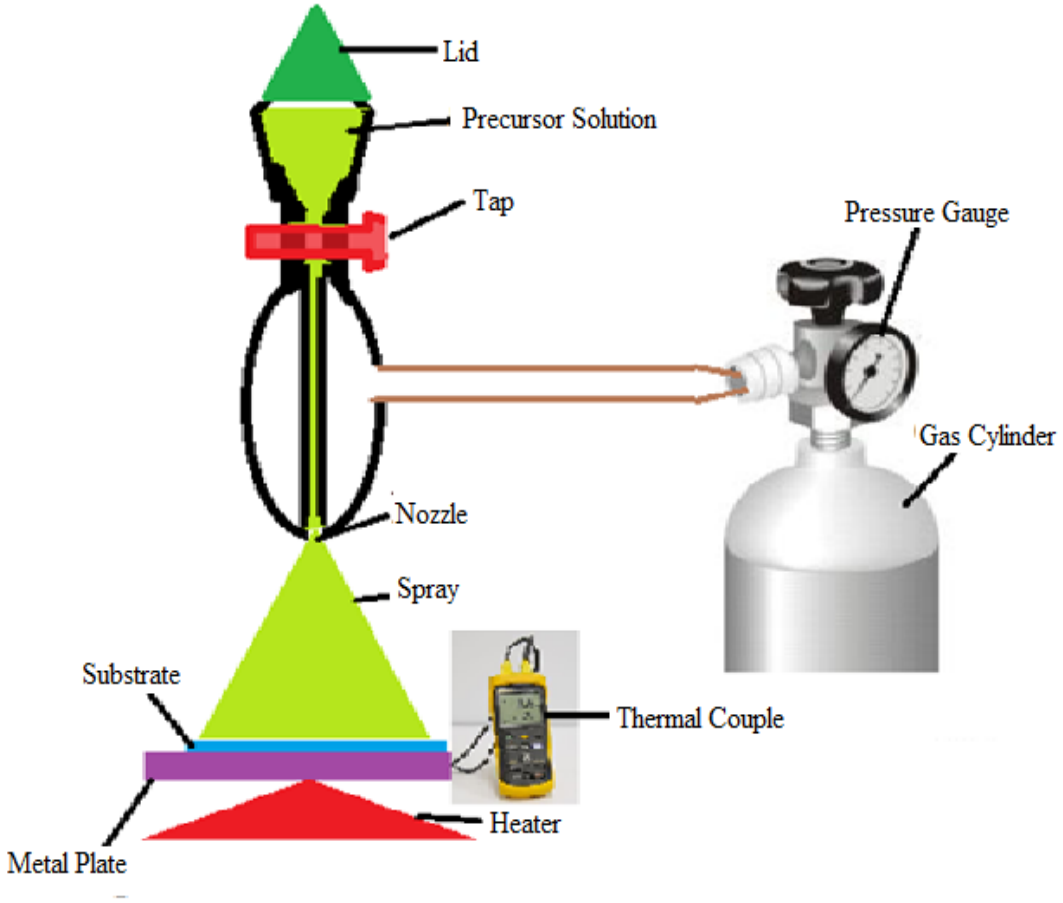

Figure 3.10: Spray Pyrolysis Setup.

3.10 Optical Characterization

The diagram shown in figure 3.11 below illustrates how transmittance and reflectance of thin films are obtained. Light energy of chosen beam intensity I_o, and wavelengths are incident on the thin film whose thickness (t) and the comparative transmission is detected. The band gap (E_g) if a factor used in measurement of transmittance and reflectance light, where energies less than the band gap are transmitted whereas those with energies greater than the E_g are absorbed. This detector also indicates the intensity of transmitted and absorbed light. Note that the quantity of absorption is dependent on the thin film thickness, thin film properties and light's wavelength.

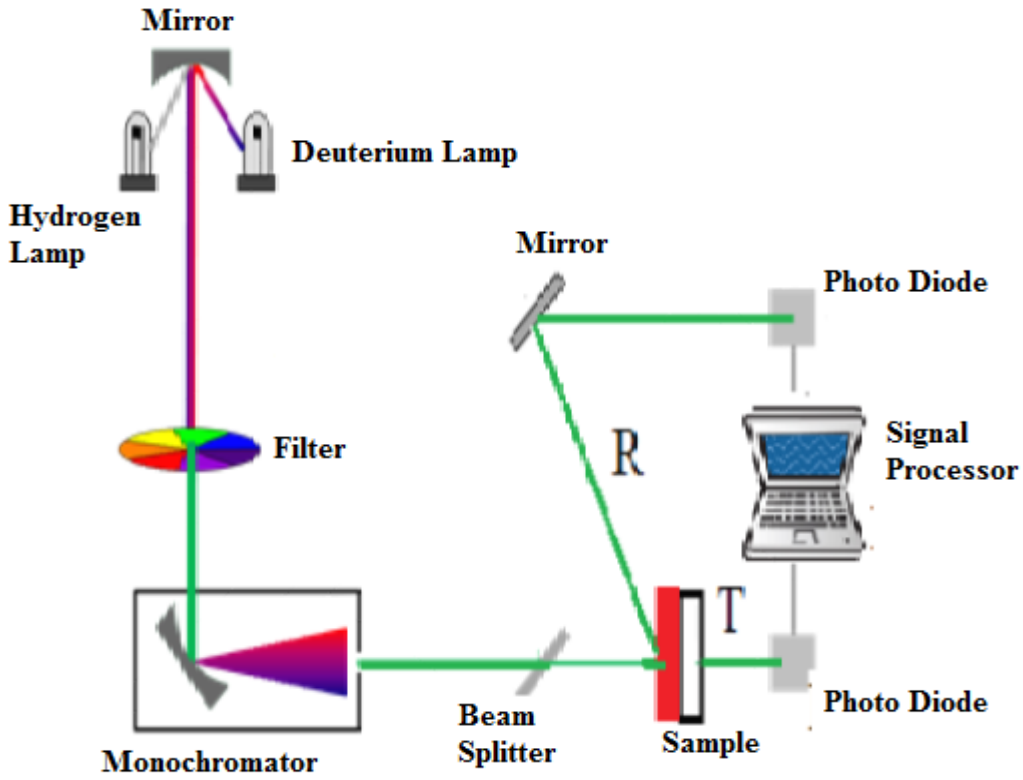

Figure 3.11: Schematic diagram for optical transmission measurements.

Equation 3.47 shown below used the absorption coefficient values to identify the Band gap:

$$(\alpha hv) = A(hv - E_g)^n \qquad (3.47)$$

where h is the Planck's constant (6.626 x 10^{-34}Js), E_g is the band gap of the material, v the frequency of light, n is an exponent with its value depending on the type of transition involved, A is the edge width parameter which is a constant and α the absorption coefficient

The film optical band gap was determined through plotting a graph of $(\alpha hv)^2$ against

hv. Extrapolating to the $hv\ axis$ the linear part of the $(\alpha hv)^2$ curve gives an estimate of the Band gap.

The transmitted light intensity, I_t, passing through a layer of thickness l, is expressed as:

$$I_t = I_0 e^{-\alpha l} \qquad (3.48)$$

Rearranging equation 3.48 we get an expression for α as follows:

$$\alpha = \frac{1}{l} In \left[\frac{I_0}{I_t}\right] (Cm^{-1}) \quad (3.49)$$

Calculation of Transmittance of the thin film was done using;

$$\text{Transmittance } (T) = \frac{I_t}{I_o} \quad (3.50)$$

A beam of monochromatic light of sufficient energy, known frequently and intensity was shone onto the thin film. The detector was used to measure the intensity of the reflected light. The following equation gives the numerical value of reflectance.

$$\text{Reflectance } (R) = \frac{I_R}{I_o} \quad (3.51)$$

Where I_R is the reflected intensity and I_o is the incident intensity of the beams.

CHAPTER 4

MATERIALS AND PROCEDURE

4.1 Introduction

The characterization of Sn_xSe_y and 0-10% Ni doped SnO_2 thin films and their preparation by Spray Pyrolysis is presented in this chapter. The electrical properties of the discrete thin films was achieved using Four Point Probe method mounted on Keithley 2400 Source Meter and optical properties were studied using Solid Spec 3700 DUV spectrophotometer as shown in Figure 4.1. Fabrication of Sn_xSe_y-SnO_2: Ni P-N junction was done by first depositing 2% Nickel doped SnO_2 layer on a glass substrate followed by deposition of Sn_xSe_y of ratio 1:1. The Aluminium back contact was finally fabricated on the P-N junction, then electrode was fixed. The Solar Cell simulator was used to obtain the I-V characteristics data.

Figure 4.1: Pictoral figure UV-VIS-NIR 3700 DUV (Shimadzu) Spectrophotometer

4.2 Cleaning the Substrate

The slides were first soaked in water containing soap and sonicated for about 30 minutes. Distilled water was used to rinse the slides. After rinsing, the slides were submerged in distilled

water and sonicated for a further 30 minutes. The slides were rinsed using distilled water and then left to dry. The glass slides were kept in a desiccator after drying. They were hence ready for thin film deposition.

4.3 Precursor Preparation and deposition of Nickel doped SnO_2

Precursor solution was prepared using a 0.05M Tin (II) Chloride ($SnCl_4.2H_2O$) mixed with 0.05 M Nickel chloride 6-hydrate ($NiCl_2.6H_2O$) in distilled water and then ethanol in the ratio 1:1 to get equal proportions or to obtain a consistent balance of water and ethanol, then soaked in an ultrasonic bath (300 W and 60 kHz) for about 10 minutes. The solution was left for a week for complete dissolution. The solution acquired was SnO_2: Ni.

Molar masses were used to calculate the percentage of dopant in SnO_2: Ni solution. The deposition conditions for the films were; substrate temperature of 375^0C, solution flow rate of 6ml/min, a gas pressure of 4.5×10^5 Pa, Nozzle-Substrate height of 20cm and carrier gas was argon gas to form SnO_2: Ni thin films. This was achieved using Spray Pyrolysis method. For optimization electrical and optical characterization of the films was done.

Table 4.1: Deposition parameters of SnO_2: Ni thin films

Parameter	**Units**
Solution flow rate	6 ml/min
Ni doping	0, 2, 4, 6 , 8, 10%
Deposition temperature	375^0C
Gas pressure	Argon gas; 4.5×10^5 Pa
Volume sprayed	30 ml
Nozzle-Substrate height	20.0 cm

4.4 Precursor Preparation and deposition of Sn_xSe_y

Tin monoselenide was prepared using precursor compounds which include 0.05M 1, 1-dimethyl-2-selenourea ($C_3H_8N_2Se$) compounds and 0.05M $SnCl_2.2H_2O$ mixed with distilled water and isopropyl alcohol in a ratio of 1:3. Molar masses were used to calculate the ratios of Sn_xSe_y. The ratios were 0.4, 0.6, 0.8, 1.0, 1.2, and 1.4. The films with different ratios of Selenides in the solutions were fabricated on a glass substrate under fixed deposition conditions. The deposition conditions for the films were; substrate temperature of 375^0C, solution flow rate of 8ml/min, a gas pressure of 4.5×10^5 Pa, Nozzle-Substrate height of 20cm and carrier gas was argon gas to form SnSe thin films. This was achieved using Spray Pyrolysis method. Optimization was achieved by characterizing the optical and electrical properties of the films.

Table 4.2: Deposition parameters of SnSe thin films

Parameter	**Units**
Solution flow rate	8 ml/min
Sn_xSe_y sample ratios	0.4, 0.6, 0.8, 1.0, 1.2, 1.4
Deposition temperature	375 ^{0}C
Gas pressure	Argon gas; 4.41×10^5 Pa
Volume sprayed	32 ml
Nozzle-Substrate height	20.0 cm

4.5 Spray Pyrolysis and Experimental Parameters

Deposition of the thin films was done using the spray pyrolysis technique. To produce SnO_2, Ni: SnO_2, Sn_xSe_y and Sn_xSe_y: Ni-SnO_2 films, the solution was sprayed onto a pre-heated glass

substrate at a temperature of 375^{o}C using compressed air for the atomization of the precursor. At the heated surface, different types of ions in thermal motion was attracted or repelled under the action of electric forces. The more stable chemical composition will be crystallized on the substrate (Jebbari *et al.*, 2010). The growth of a thin layer neutral and well crystallized was then observed.

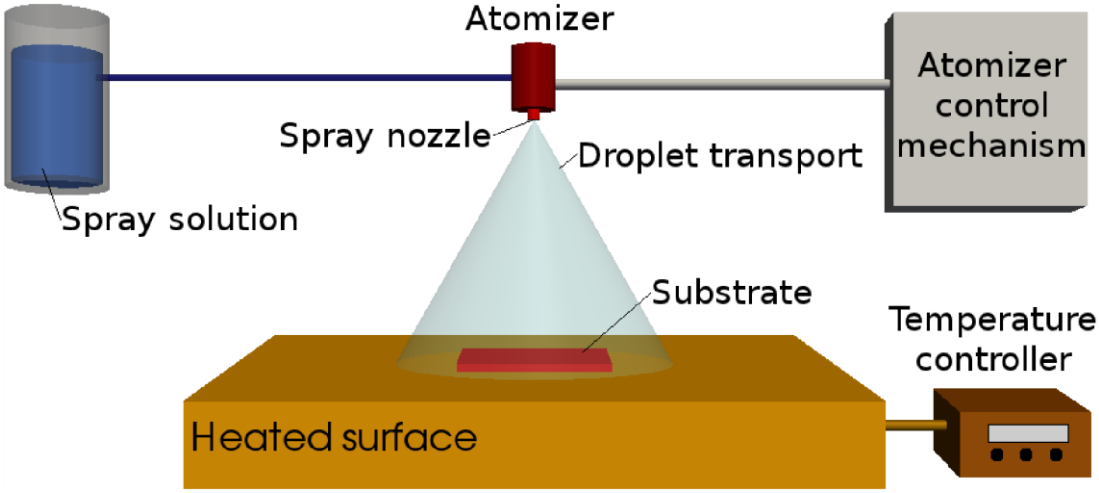

Figure 4.2: General schematic of a spray pyrolysis

4.6 Electrical Characterization

Measurement of the prepared thin films was done using the four point probe method (Figure 4.3). Keithley 2400 Source Meter measured the sheet resistivity using the four contact terminals at each corner of the thin film. As shown in the figure 4.4 the SnO_2, Ni- SnO_2, Sn_xSe_y and Sn_xSe_y: Ni-SnO_2 thin films should be square in geometry.

Figure 4.3: A photograph of Keithley Source Meter 2400 model

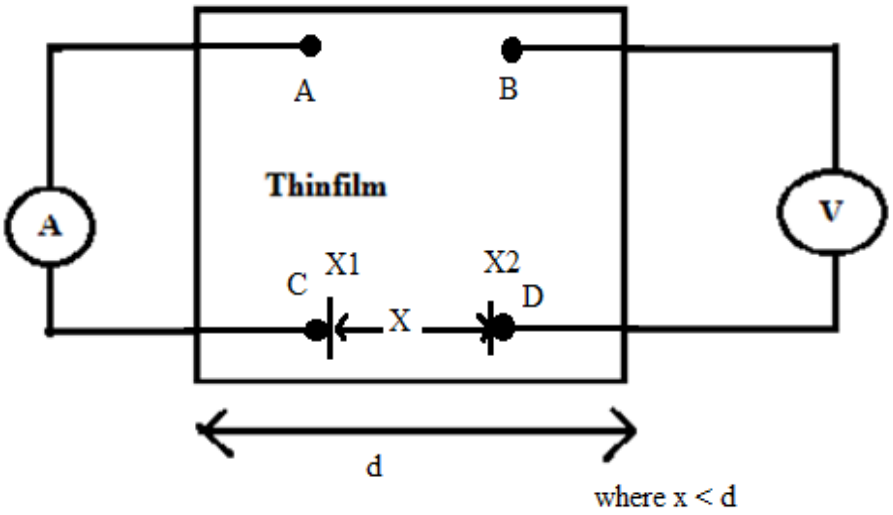

Figure 4.4: Arrangement used to measure sheet resistivity and its schematic diagram.

4.7 Optimized deposition parameters

Optimized parameters were recorded in table 4.3 after several trial deposition of thin films of Sn_xSe_y and SnO_2: Ni, to ensure more efficient solar cell.

Table 4.3: Summarized optimized deposition parameters for Sn_xSe_y and SnO_2: Ni thin films

Tin Selenide (SnSe)		Nickel doped Tin Oxide (SnO_2:Ni)	
Substrate	Microscope slide at 648 K	Substrate	Microscope slide at 648 K
Deposition pressure	4.41×10^5 Pa	Deposition pressure	4.5×10^5 Pa
Sn:Se Ratio	1:1.0	Doping level	2%
Band gap	1.39 eV	Band gap	3.74 eV
Sheet resistivity	33.62 Ωcm	Sheet resistivity	43.33 Ωcm

4.8 Fabrication of SnSe-SnO_2: Ni p-n Junction

The solar cell device geometry was fabricated in the format constituting glass/ SnO_2: Ni/SnSe/Al in steps outlined below.

- The n-type layer of transparent conducting SnO_2: Ni film was deposited first on to a glass substrate at a temperature of 648K and pressure of 4.5×10^5 Pa by Spray Pyrolysis technique.
- A p-type layer of $SnSe_{1.0}$ was deposited on to SnO_2: Ni on the same substrate at the same temperature and pressure of 4.41 x 10^5 Pa by Spray Pyrolysis technique.
- Fabrication was completed by depositing Aluminium back contact of area $1cm^2$ on $SnSe_{1.0}$ film. The thin film obtained was $SnSe_{1.0}$- SnO_2: Ni which formed the p-n heterojunction.

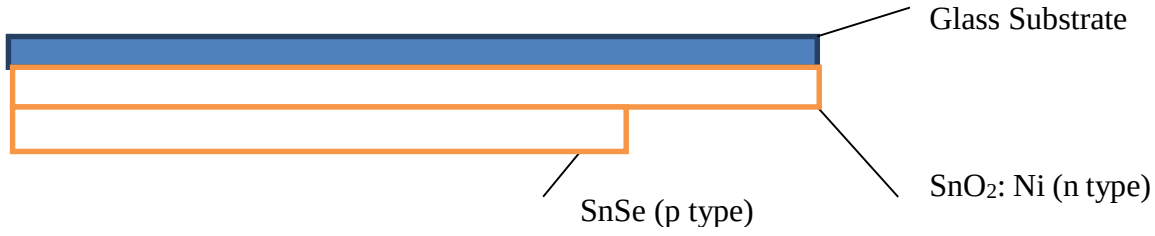

Figure 4.5: Schematic diagram of SnSe-SnO_2: Ni p-n Junction.

4.8.1 Characterization of SnSe-SnO_2: Ni solar cell

The set up for measuring the diode characteristics is shown in the figure 4.6 below.

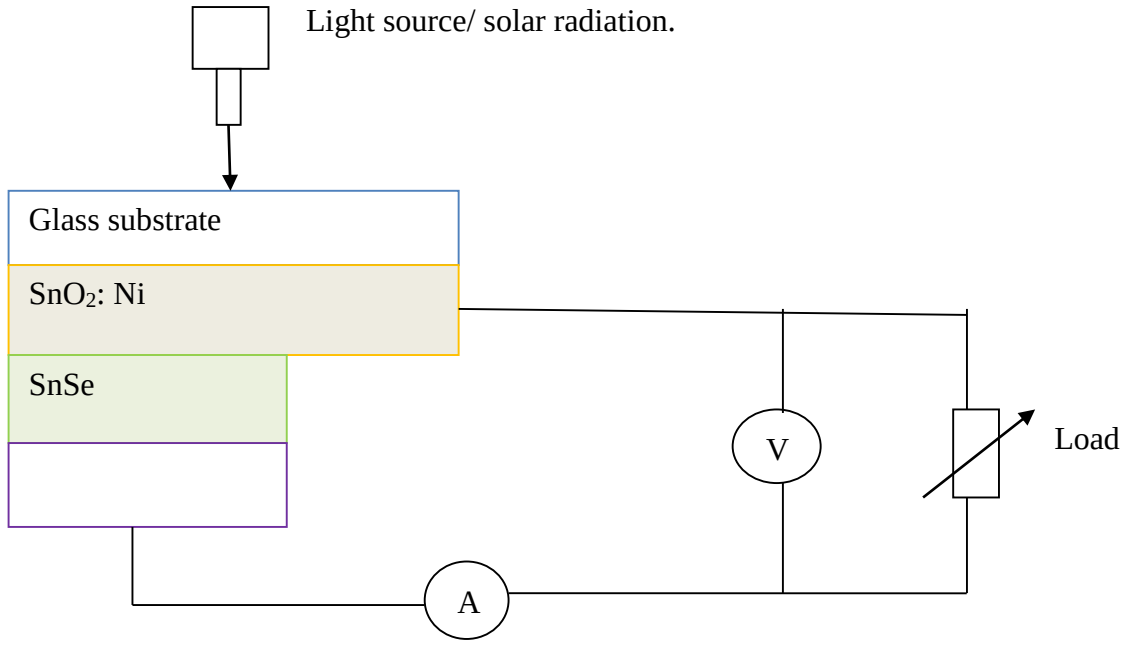

Figure 4.6: I-V characteristics of a p-n Junction measurement circuit schematic diagram.

I-V analysis was done using high voltage Keithley 2400 series source meter. A solar simulator as shown on figure 4.7 that used halogen lamp was used for illumination which was made from OSRAM where optoelectronic products are designed. The set up and connection to the solar cell is shown above. The I-V curves under illumination were obtained.

Figure 4.7: A pictorial figure showing a solar simulator

CHAPTER 5

RESULTS AND DISCUSSION

5.1 Introduction

The electrical and optical results of SnSe and SnO_2: Ni thin films studied are given and discussed. Optical and electrical properties are used as basis for optimizing Sn_xSe_y and SnO_2: Ni thin films for fabrication of the Sn_xSe_y - SnO_2: Ni p-n junction. The I-V characteristics response of Sn_xSe_y - SnO_2: Ni was used to determine short circuit current, open circuit voltage, fill factor and the efficiency of the solar cell.

5.2 Optical spectra of thin films

3700 DUV UV-VIS-NIR Spectrophotometer was used to obtain the experimental data for transmittance and reflectance using the software of UV probe. Microsoft excel converted the data in its format from which spectra graphs were plotted separately for both tin selenide and Nickel doped Tin Oxide thin films using Microcal Origin 8.

5.2.1 Tin-Selenide (Sn_xSne_y)

5.2.1.1 Transmittance spectra of tin selenide (Sn_xSe_y) thin films

Spectra of transmittance of Sn_xSe_y thin films depended on ratios of their masses. The average transmittance spectra for Sn_XSe_Y samples at different ratios is shown on figure 5.1. The graphs shows that average transmittance were below 65% in the visible range (400nm-780nm). As wavelength of incident photon increases, it is observed that transmittance also increases. This was due to low absorption as a result of low energy of photons lower than the band gap.

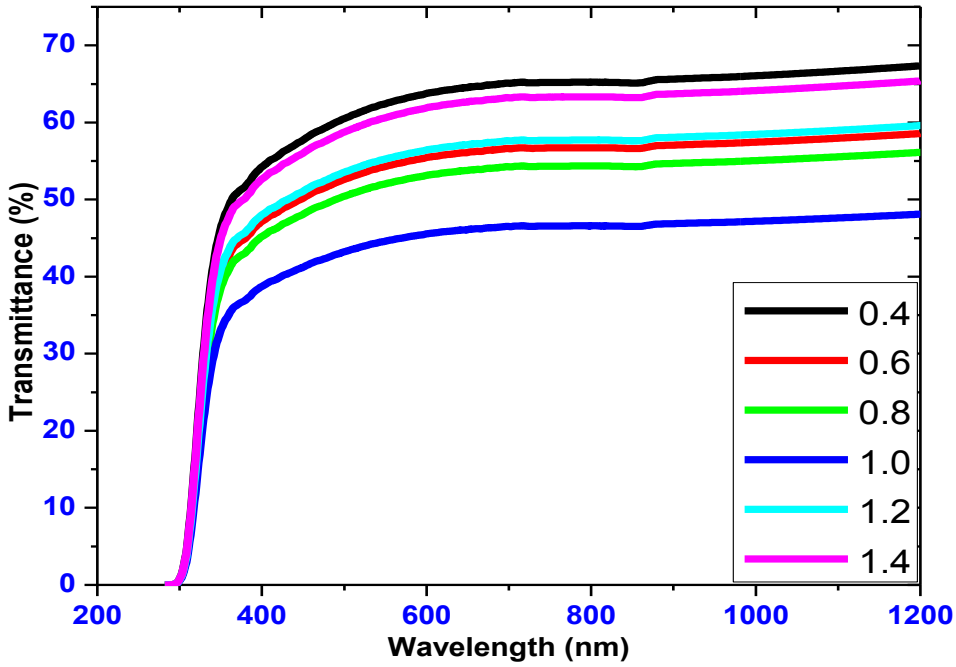

Figure 5.1: Transmittance spectra against wavelength for Sn_xSe_y in various ratios.

A slight increase in transmittance beyond the visible range (> 750nm) was observed then gradual increase in transmittance was observed above 780nm. This could be associated with low energy of photon making absorption to be low. The transmittance increased as the ratio of Sn:Se approached the stoichiometric values. Transmittance decreased with increase in selenium ratios and after attaining a ratio of 1:1 it again increased. This was attributed to the decrease in films band gap with increasing ratios which further increased after a ratio of 1:1. This shows that a ratio of 1:1 had the highest absorption which was a best material for p type semiconductor.

5.2.1.2 Reflectance spectra for tin selenide (Sn_xSe_y) thin films

Spectra of optical reflectance of tin selenide with wavelength is shown in figure 5.2. The graph shows that the average reflectance within the visible region was less than 10% for all the tin-

selenide samples, indicating that the film had high absorption making the film good as an absorber layer.

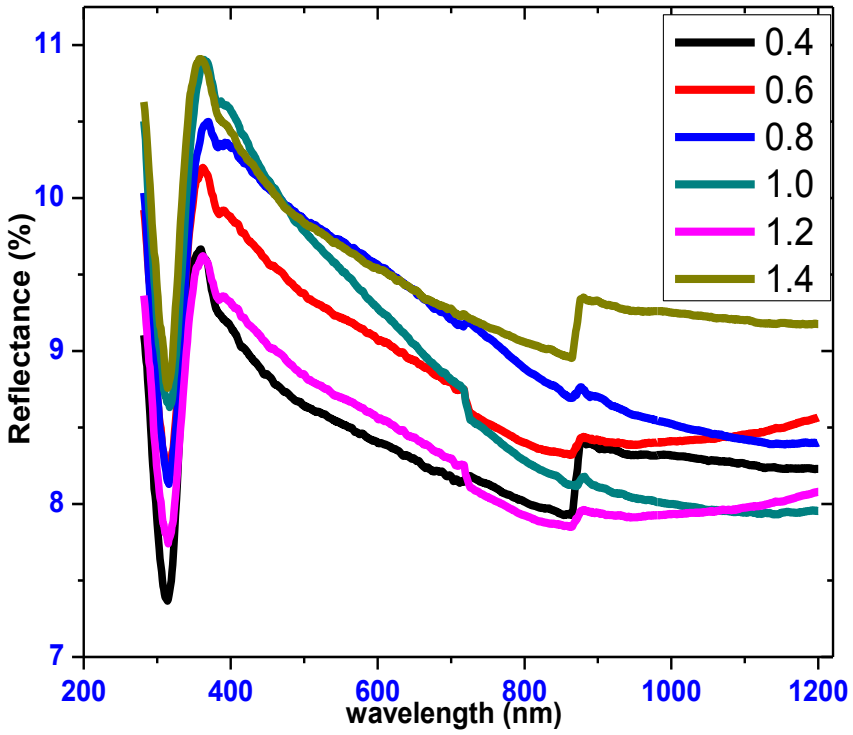

Figure 5.2: Optical reflectance spectra of tin selenide in various ratios.

The thin films are good absorbers of photon energy as evidenced from their low reflectance that can create more electron-hole pairs.

5.2.1.3 Absorbance spectra for tin selenide (Sn_xSe_y) thin films

Figure 5.3 shows spectra of optical absorbance of tin selenide with wavelength. The absorbance decreases with increase in wavelength. At lower wavelengths the photons has high energy compared to the band gap energy hence a lot of it is absorbed. SnSe ratio of 1:1 has the highest absorbance of an average of 46.26% in VIS region making it a good absorber layer.

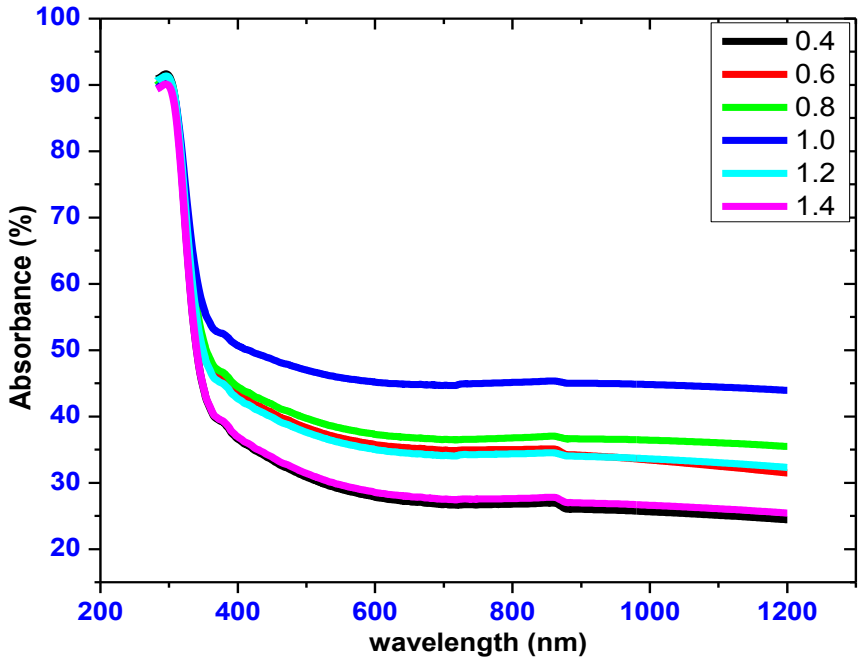

Figure 5.3: Optical absorbance spectra of tin selenide in various ratios.

5.2.1.4 Absorption coefficient for tin selenide (Sn_xSe_y) thin films

Absorption coefficients at different ratios for tin selenide with varying wavelength from 280 nm to 1200 nm is shown on figure 5.4. From the curves, at lower wavelengths high absorption coefficients were observed for the different tin-selenium samples. For all the samples the average absorption coefficient within the visible range (400-780) nm increases with increasing tin-selenium ratio up to a ratio 1:1 and then decreases. The Sn:Se gave an average absorption coefficient $> 10^5$ cm^{-1} thus making it a dependable material for casting a good absorber layer for solar cells (Porortmans & Arkhipov, 2006). Electrons in the valence band absorbs the photons and excited into the conduction band and it is more pronounced on the materials with higher absorption coefficients.

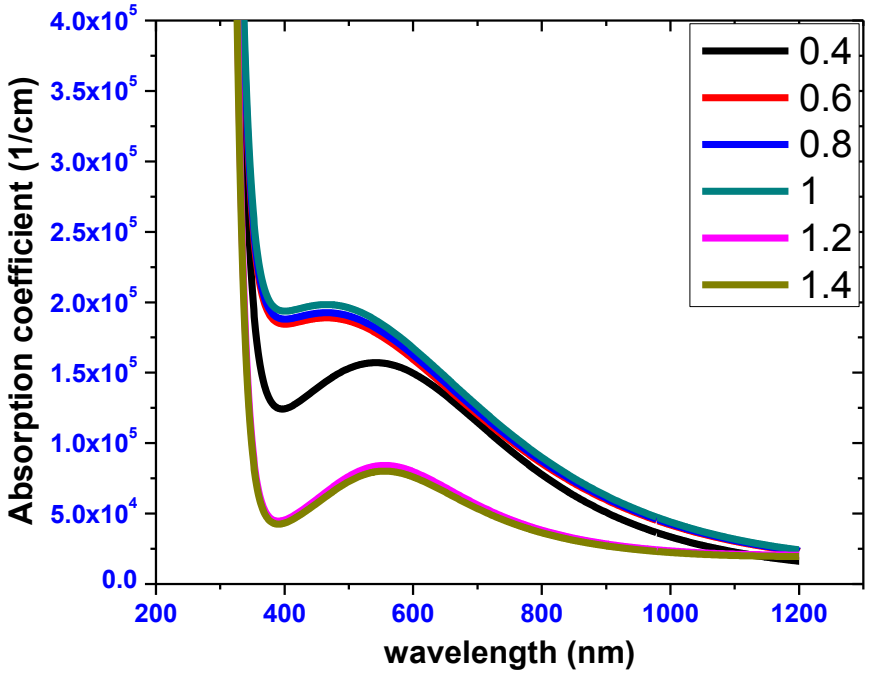

Figure 5.4: The absorption coefficient for different tin selenide ratios versus wavelength.

5.2.1.5 Extinction coefficient for tin selenide (Sn_xSe_y) thin films

Figure 5.5 shows the dependence of extinction coefficient with wavelength. As the tin selenide ratios increases, extinction coefficient increases with the film of ratio 1:1 recording the highest extinction coefficient which implies that its rate of absorption is good. After that extinction coefficient decreases. Extinction coefficient is a measure of light in the film lost due to absorption and scattering as it penetrate through material. Complex refractive index relates refractive index n and extinction coefficient k by a connection $n^* = n - ik$ and for this instance k is implied as the damping factor of a material.

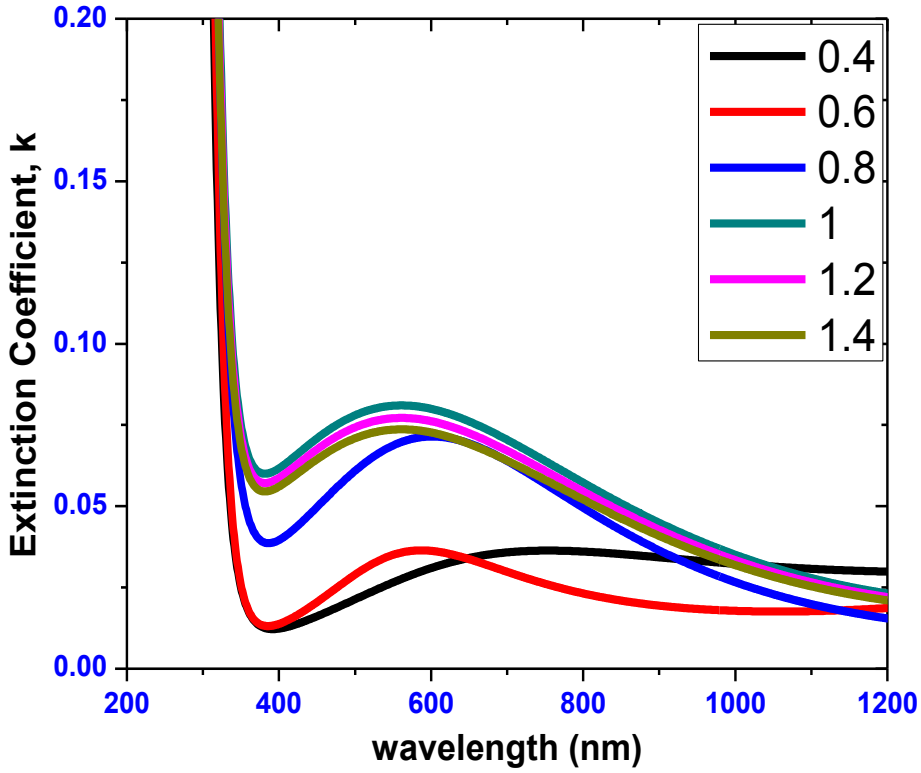

Figure 5.5: Extinction coefficient against wavelength of SnSe thin films for various tin selenide ratios.

5.2.1.6 Refractive index for tin selenide (Sn_XSe_Y) thin films

The variation of refractive index of Sn_xSe_y thin films with wavelengths is shown on figure 5.6. As wavelength increases, it is observed that the refractive index decreases. Important to note is that a ratio of SnSe as the highest refractive index implying that it is a good absorber material this is because the radiation takes a longer time through the film using,

$$n = \frac{c}{v}. \qquad (5.1)$$

Where c is the speed of light c = 2.998×10^8 ms^{-1} , n is the refractive index and v the speed of light in a medium.

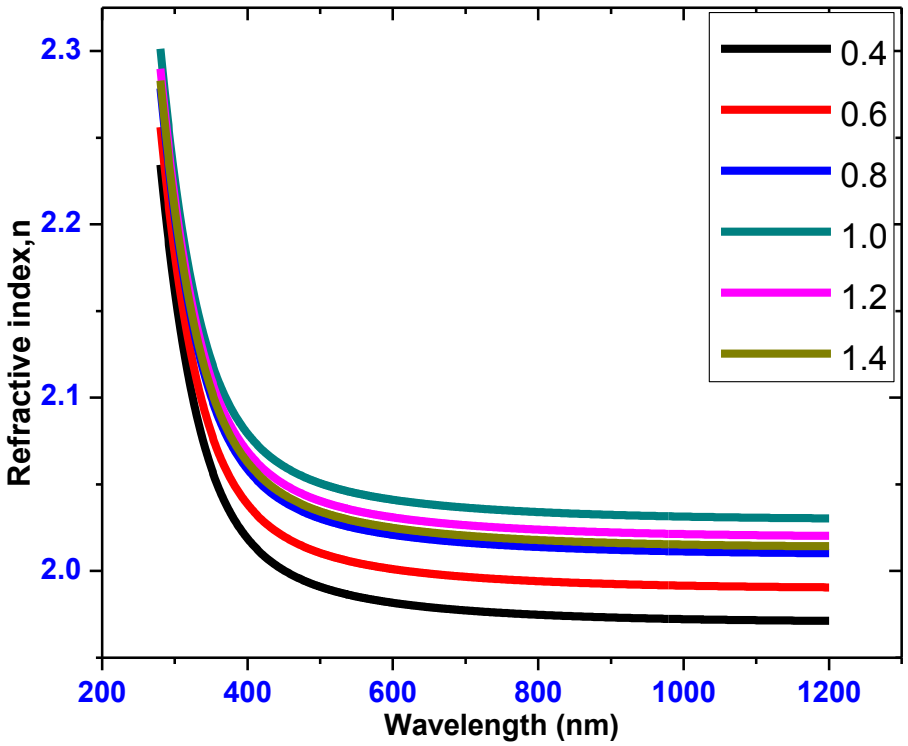

Figure 5.6: Refractive index versus wavelength of SnSe of varying ratios.

5.2.1.7 Averages of transmittance, absorbance and reflectance in VIS region of Sn_xSe_y.

Figure 5.7 shows how averages of transmittance, absorbance and reflectance of SnSe thin films varied with Sn_xSe_y ratios within visible region. It is clearly seen a sample of ratio1:1 has the highest absorbance. Table 5.1 shows that average transmittance for all the samples in VIS region was below 65%, reflectance for all the samples was below 10% and absorbance below 50%. A sample of SnSe of ratio 1:1 has the highest absorbance making it a good absorber layer. Optimization of SnSe using average absorbance (%) in VIS region against sample ratios figure 5.8 shows that ratio of 0.93 has the highest absorbance.

Table 5.1: Averages of transmittance, absorbance and reflectance in VIS region of Sn_xSe_y.

VISIBLE REGION (380 – 780 nm) AVERAGES			
Sn_xSe_y (y/x)	Transmittance %	Reflectance %	Absorbance %
0.4	62.01	8.50	29.49
0.6	53.92	8.87	37.21
0.8	51.68	9.65	38.67
1.0	44.30	9.44	46.26
1.2	54.88	8.65	36.47
1.4	60.21	9.65	30.14

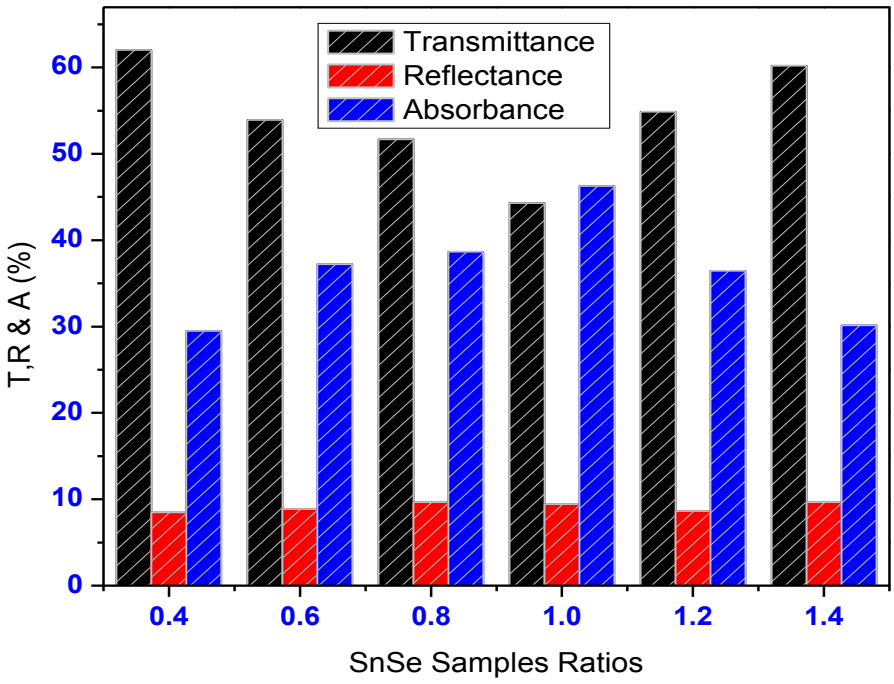

Figure 5.7: shows how averages of transmittance, reflectance and absorbance of SnSe thin films varied with ratios in visible region.

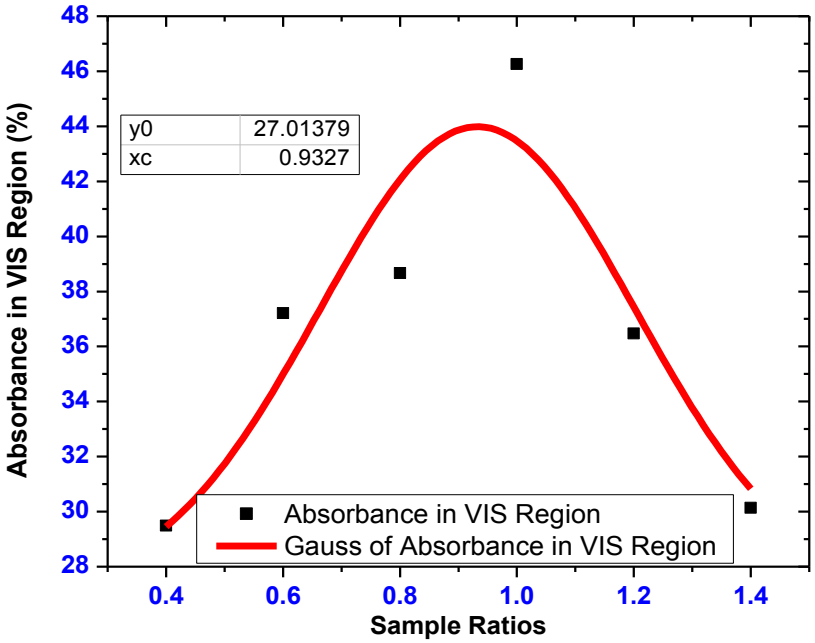

Figure 5.8: Optimization of SnSe using average absorbance (%) in VIS region against sample ratios.

5.2.1.8 Optical band gap energies for tin selenide (Sn_xSe_y) thin films

Optical band gap for various tin selenide ratios thin film samples is shown on Table 5.2. A graph of $(E\alpha)^2$ against energy drawn using data from Scout 98 programme was used to calculate the band gap energy. From the optical absorbance vs. wavelength data was obtained and using equation $(\alpha hv)^2 = A(hv - E_g)$ mathematical treatment was done to derive the transition type and the band-gap energy. For direct allowed band gap. The SnSe samples optical band gap energy rest at 1.39-2.23±0.05 eV and lowest band gap energy being found on the Sn:Se ratio of 1:1 sample. The values of band gap reported by (Kumar , 2010) for Sn_xSe_y lie between 1.18-1.85±0.05 eV and 1.18eV to 1.75eV as reported by (Nyakundi *et al.*, 2014) .

Table 5.2: Sn_xSe_y variation by mass ratio and calculated band gap energy values

Sn:Se mass ratio	Optical band gap [±0.05 (eV)]
1:0.4	1.97
1:0.6	1.82
1:0.8	1.66
1:1.0	1.39
1:1.2	1.87
1.1.4	2.23

A graph of forbidden gap energy against Sn:Se sample ratios was plotted from the data obtained above. The optimum Sn:Se thin film ratio is 1:1 simply because it depict the least forbidden gap of 1.39±0.05 eV as shown in a graph of figure 5.9 below.

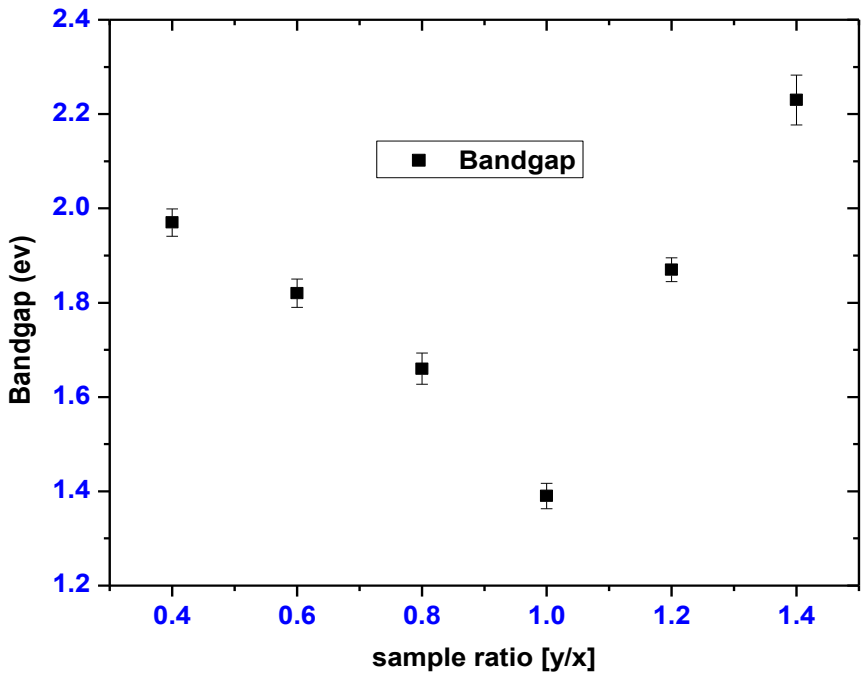

Figure 5.9: SnSe thin films of forbidden energy band gap varying with ratios.

5.2.2 Nickel doped Tin oxide (SnO_2: Ni)

5.2.2.1 Optical transmittance spectra for SnO_2: Ni thin films

Figure 5.10 shows the optical transmittance for tin doped zinc oxide at different doping percentages with wavelength. The optical transmittance of SnO_2 and Nickel doped SnO_2 was found to be above 75% in the VIS and NIR region.

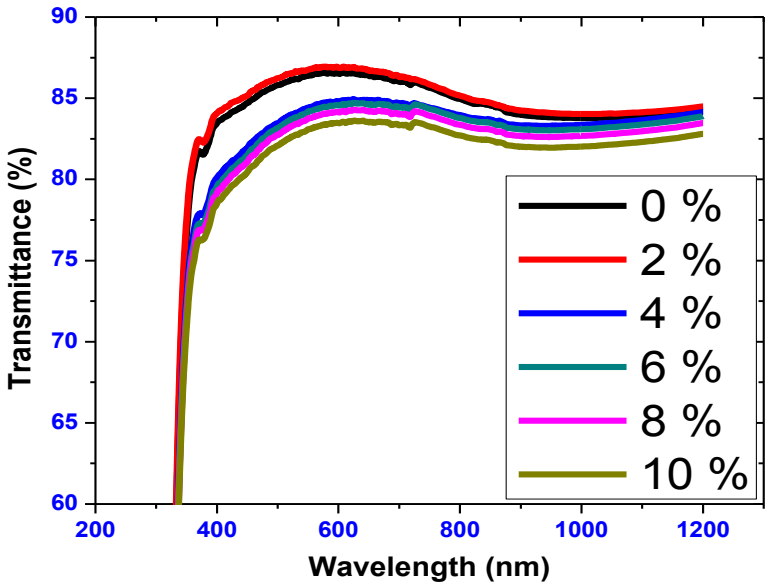

Figure 5.10: Graph of transmittance spectra of Tin oxide doped with thin Nickel Films.

As the wavelength of illuminated photon energy increases transmittance increases briskly to maximum as verified from the spectral data. Transmittance for all the samples is highest within the visible region. Transmittance decreases for photons of wavelength beyond 750nm. This is associated with the increase in optical scattering caused by rough surface morphology. Since the photon energies are less than or too close to forbidden gap of the thin films, low optical absorption takes place results to higher transmittance. Unlike other samples the 2% Nickel doped sample depicted to some extent higher transmittance which makes it a good material for a window layer. Transmittance then slightly decreases after 2 % as Nickel concentrations increased. This is attributed to free charge carriers coupling to the electric field (Shishiyanu *et al*., 2004).

5.2.2.2 Optical reflectance spectra for SnO_2: Ni thin films

The plots in figure 5.11, displays a spectra of reflectance. Reflectance was low and lying in the range of 8-10% in the infra-red region, ultra violet and visible range of the solar spectrum. For both doped and un doped SnO_2 the overall reflectance is fairly low, this makes SnO_2 doped Ni applied in photovoltaic as a suitable material for use as a window layer in applications. At around 850 nm a kink is observed, this is caused during the exchange of hydrogen lamp and Deuterium lamp (Refer to figure 3.11).

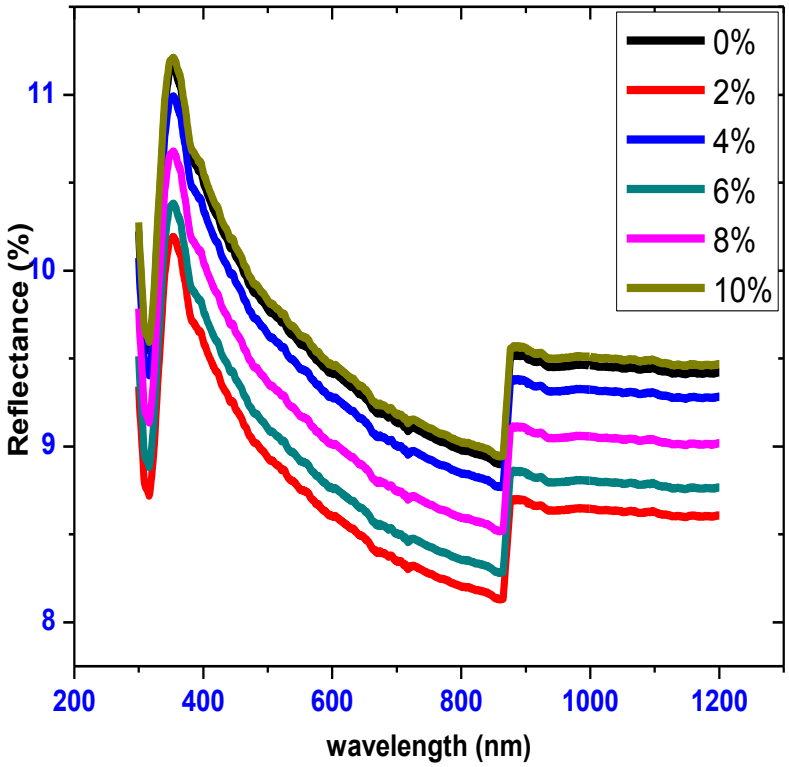

Figure 5.11: Optical reflectance spectra for Nickel doped Tin oxide

5.2.2.3 Refractive index for Nickel doped Tin oxide

Initially refractive indices decreased with wavelength from 280-325 nm as shown in figure 5.12 while there were no meaningful vicissitudes of refractive indices with increase in wavelength from 325-800 nm for un doped and doped Tin oxide. The refractive index

decreased with 2% Nickel showing the least value and then increased. This means the photons travels through the film faster hence absorption is minimal. This is likely the cause of high transmittance.

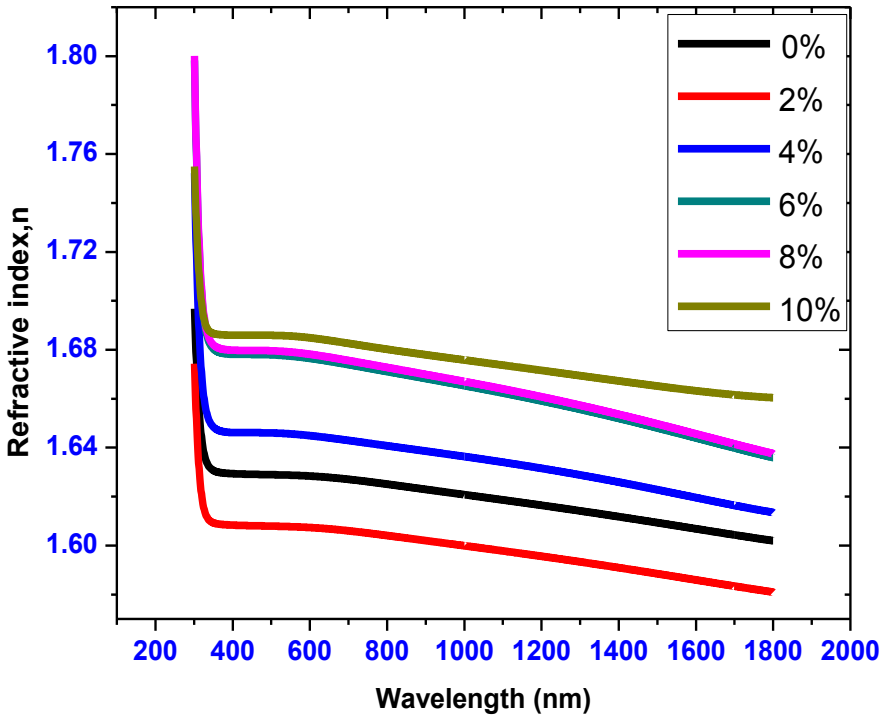

Figure 5.12: Refractive index versus wavelength for Nickel doped Tin oxide.

5.2.2.4 Absorption coefficient for Nickel doped Tin oxide

Figure 5.13 shows absorption coefficient for SnO_2: Ni samples. The SnO_2: Ni has a low absorption coefficient at high wavelengths and a high absorption coefficient at low wavelength. Absorption of illuminated photon takes place at lower wavelengths hence high absorption coefficient as seen in the figure. This occurs because at lower wavelength, photons have high energy compared to the band gap and therefore very well absorbed. There was an observed lowest average absorption for films with 2% Nickel doping concentration within the visible range. This indicated that the film is good for a window layer. At high wavelengths we observe very low absorption. This is because at high wavelengths, the photons have low energy hence

mainly transmitted since band gap energy is not exceeded.

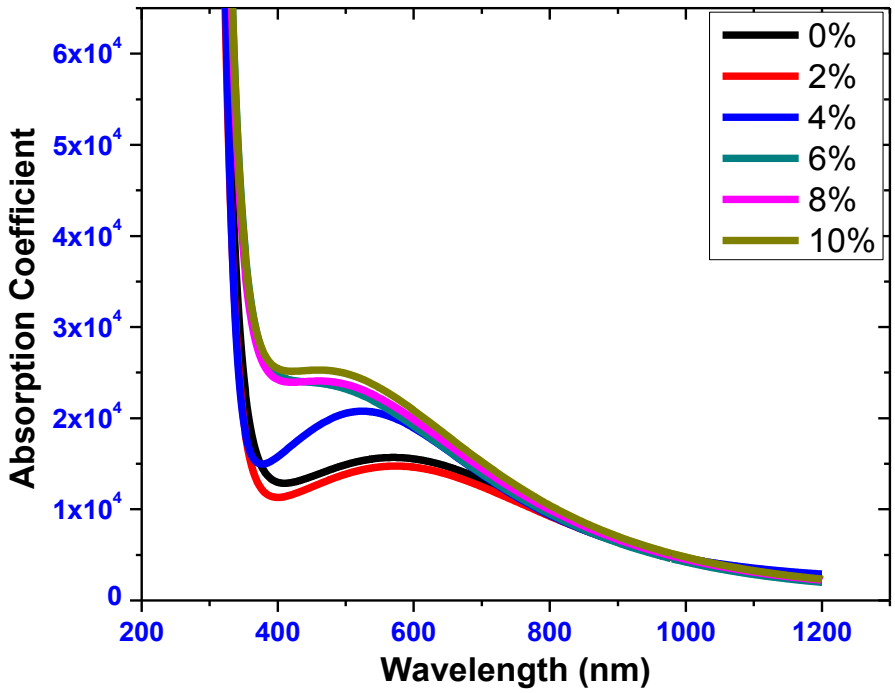

Figure 5.13: Absorption coefficient versus wavelength for Nickel doped Tin Oxide.

5.2.2.5 Extinction coefficient for Nickel doped Tin oxide

Figure 5.14 shows the extinction coefficient versus wavelength. The average extinction coefficient within the visible range was below 0.2. This indicates that Nickel doped Tin oxide is a good window layer for solar cell. The extinction coefficient is to a great extent increased at low wavelengths (< 350nm). This indicates that at low wavelengths, the films have high absorption. As well, the extinction coefficient is also decreased at higher wavelength (>750nm), this implies that the material became almost transparent at higher wavelengths. A measure of the diminution rate of transmitted light through absorption and scattering in a material is the extinction coefficient. A film of 2% has the lowest extinction coefficient in the visible region making it a good window layer.

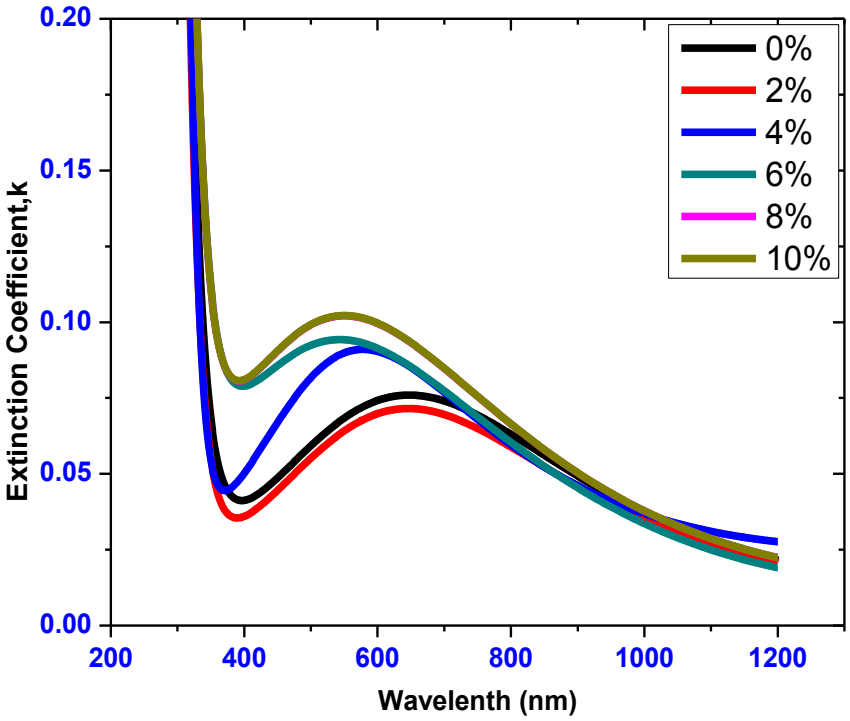

Figure 5.14: Extinction coefficient versus wavelength for Nickel doped Tin Oxide.

5.2.2.6 Averages of transmittance, absorbance and reflectance in visible region for Nickel doped Tin oxide

Figure 5.15 shows how averages of transmittance, reflectance and absorbance of Nickel doped Tin oxide thin films varied with Nickel concentration in visible region. It is clearly seen in figure 5.15 a sample of 2% Nickel has the highest Transmittance. Table 5.2 shows that average transmittance in VIS region is above 80% whereas reflectance and absorbance are below 10% for the samples. This makes these samples better window layers. Optimization of Nickel doped Tin oxide using average transmittance (%) in VIS region against Nickel concentration (%) is shown on figure 5.16 and obtained as 2.02%. This is in close range with the 1.5% Ni doped SnO_2 optimized by Chuah (2012).

Table 5.3: Averages of transmittance, absorbance and reflectance in visible region for Nickel doped Tin oxide.

VISIBLE REGION (380 – 780 nm) AVERAGES			
SnO_2: Ni (Ni %)	Transmittance %	Reflectance %	Absorbance %
0	8581	9.58	4.62
2	86.20	8.75	5.05
4	85.83	8.43	5.74
6	83.54	8.91	7.56
8	83.12	9.17	7.71

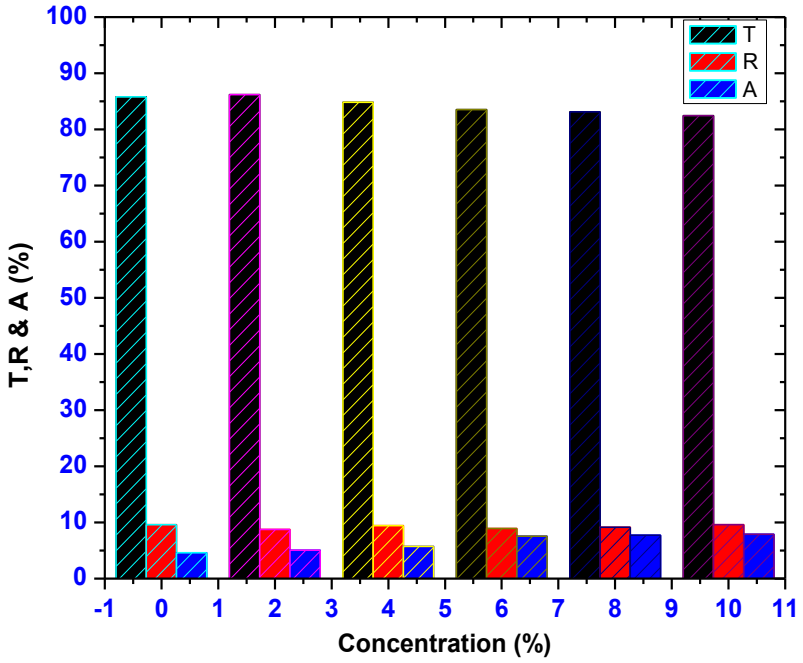

Figure 5.15: shows how averages of transmittance, reflectance and absorbance of Nickel doped Tin oxide thin films varied with ratios in visible region.

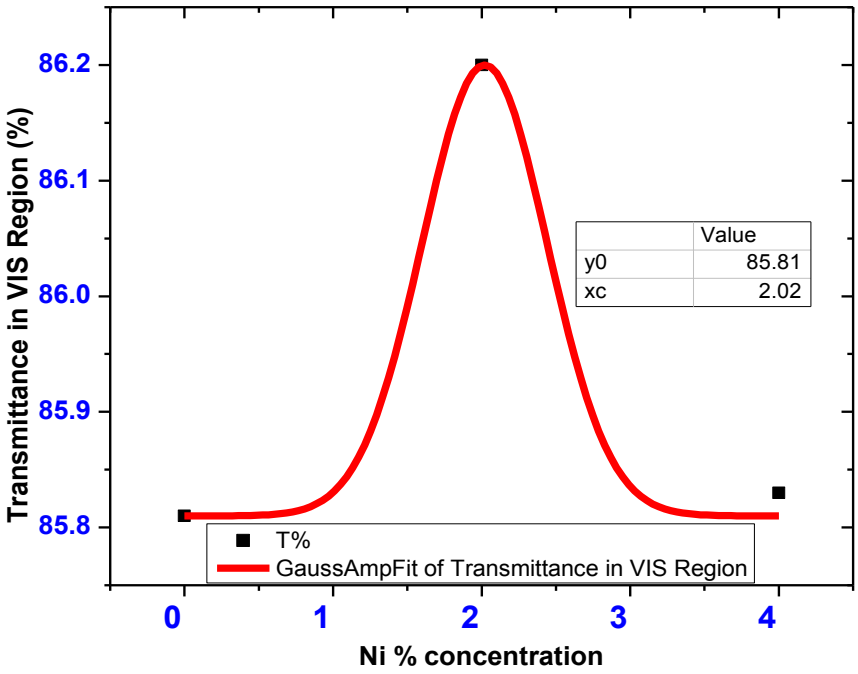

Figure 5.16: Optimization of Nickel doped Tin oxide using average transmittance (%) in VIS region against Nickel concentration (%).

5.2.2.7 Optical band gap energies for Nickel doped Tin oxide

The band gap energy values for Nickel doped Tin oxide were calculated by the scout 98 program that was used in simulation. Using the mathematical treatment of the data the transition type and the band-gap energy can be derived from the optical absorbance against wavelength using relation:

$$(\alpha hv)^2 = A(hv - E_g) \qquad (5.2)$$

Since Nickel doped Tin oxide is a direct allowed band gap. Figure 5.14 shows how to obtain the band gap using Tauc relation. When a linear graph is drawn the band gap of the sample is obtained at a point where the line cuts the energy axis.

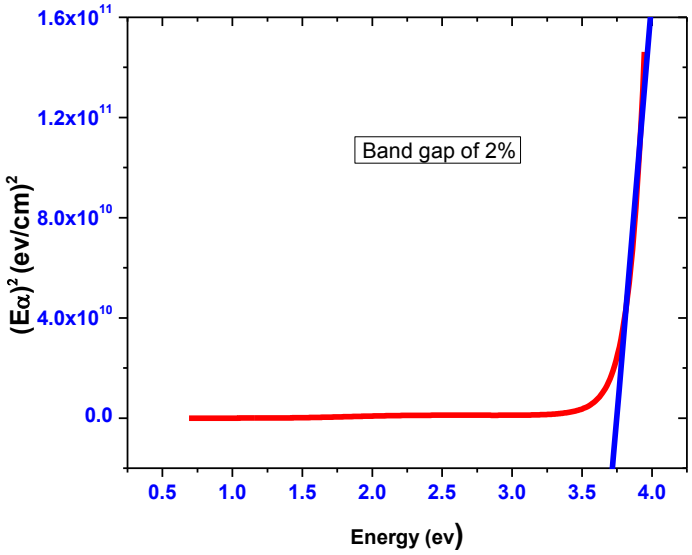

Figure 5.17: A graph showing how to obtain the band gap for Nickel doped Tin oxide using Tauc relation equation 5.2.

Table 5.4: Nickel doped Tin oxide and calculated band gap energy values.

Doping of SnO_2 with Nickel (%)	Band gap energy [±0.05 (eV)]
0.0	3.707
2.0	3.745
4.0	3.712
6.0	3.701
8.0	3.682
10.0	3.652

The range of the energy band gap of Nickel doped Tin oxide is between 3.65-3.75 eV. Kuppan *et al*., (2014) reported the energy band gap of Nickel doped Tin oxide values to lie between 3.70 eV and 3.76 eV. The optical band gap energy with doping concentration variation is depicted on a graph in figure 5.18 below.

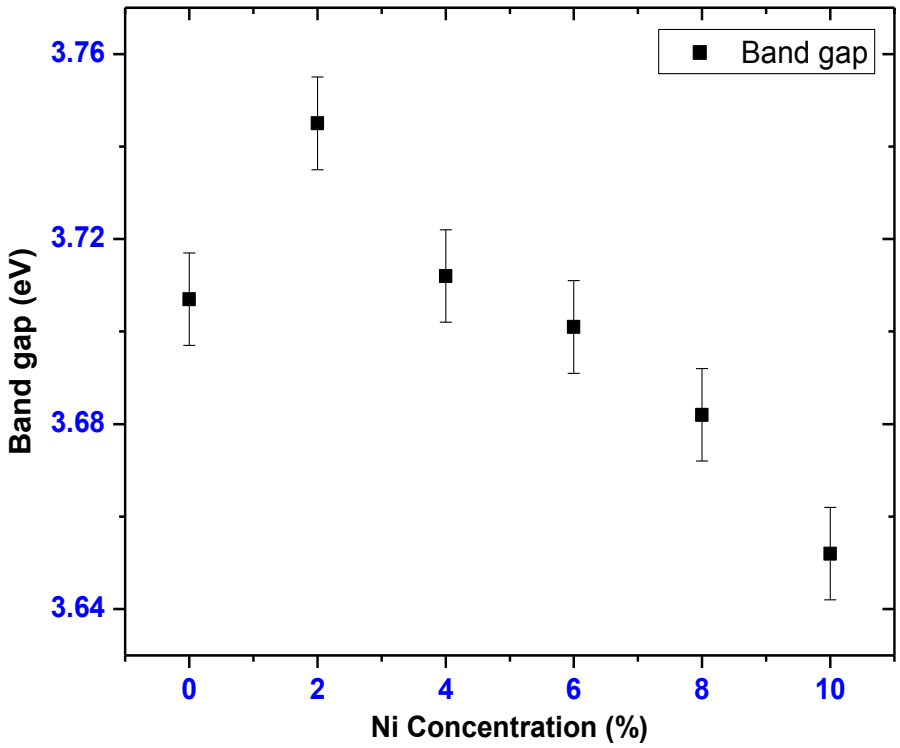

Figure 5.18: Graph of band gap energy with varying doping concentration.

In the range of 0-2 % Ni doping, increase of band was noted which is associated with the combined effect of Burstein-Moss effect and band gap narrowing (Ajimsha, 2011). When the conduction band edge density of states is exceeded by carrier concentration, this effect that occurs which match to degenerate doping in semiconductors. More and more donor states are wrought as the doping level concentration increases which slightly shift Fermi level in higher energy. From 2-10% Ni doping there is decrease in forbidden gap attributed to creation of new donor levels in the band gap due to the shift in the Fermi level therefore change in the band structure of the films.

5.3 Electrical properties of the thin films

Sheet resistivity was determined using four point probe for as prepared thin films (Agumba,

2010) computer Interfaced and mounted on Keithley 2400 source meter using LabVIEW.

5.3.1 Electrical resistivity for Tin Selenide

Electrical resistivity for tin selenide films was measured using a four point probe (Agumba, 2010). The data collected tabulated as shown in table 5.3.

Table 5.5: The variation of sheet resistivity and conductivity with the ratio of tin to selenium.

Sn:Se mass ratio	Sheet resistivity (± 0.005 Ωcm) x 10^{1}	Conductivity (± 0.005)Ωcm^{-1} x 10^{-2}
1:0.4	3.932	2.5
1:0.6	3.822	2.6
1:0.8	3.516	2.7
1:1.0	3.362	3.0
1:1.2	3.27	3.1
1:1.4	2.886	3.5

Table 5.5 shows the calculated sheet resistivity for different SnSe ratios. It was noted that sheet resistivity reduced with upsurge of selenium in tin from 39.32 $\Omega\, cm$ to a minimum of 28.82 Ωcm which is in the range of a semiconductor at room temperature ranging 10^{-1} to $10^{9}\,\Omega$ cm (Shimura, 1989). This is featured as a result of high carrier concentration and carrier mobility as associated with the film. Likewise, there is creation of fewer nucleation centres at high temperatures which bring about large crystallites size, this makes inter crystalline barriers to reduce and in the end lower the electrical resistivity. Improvement in the crystallinity of the SnSe films as well leads to decrease in resistivity at higher deposition temperature which escalates the free carrier density and the drift mobility of the charge carriers (Kumar *et al*., 2012). Conductivity increases, a behavior correlated to the enlargement of the grain size that

brings about an upsurge in carrier mobility (Martinez *et al*., 2013). Figure 5.19 shows a graph of sheet resistivity versus SnSe films of different ratios.

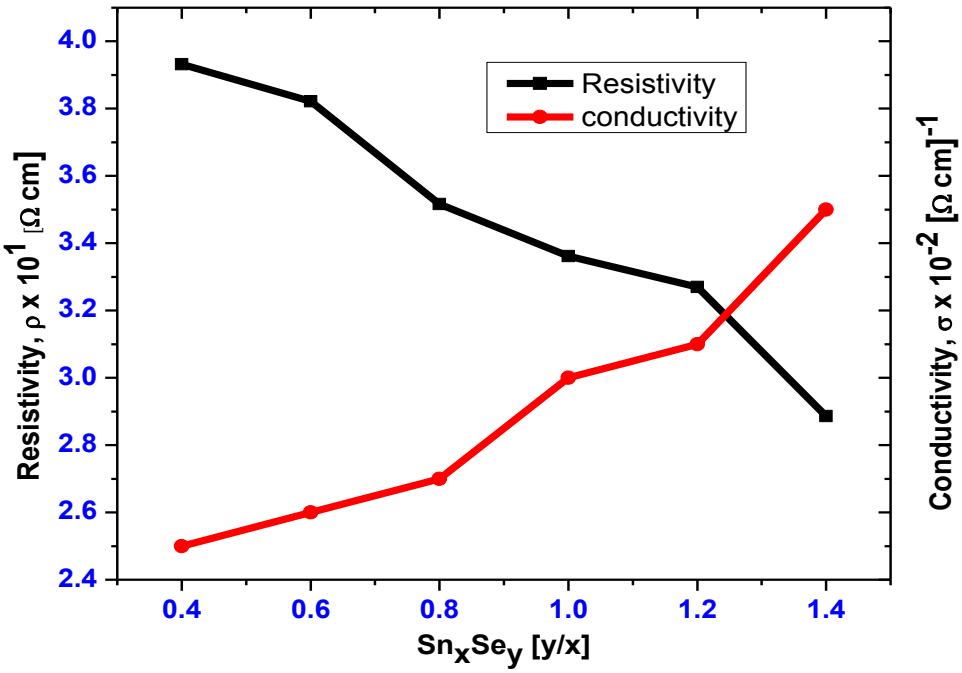

Figure 5.19: Variation of sheet resistivity at different tin to selenium ratio.

5.3.2 Electrical resistivity for Nickel doped Tin oxide

Electrical resistivity of SnO_2: Ni as prepared for various doping concentrations were measured using a four point probe (Agumba, 2010). The data collected was tabulated as shown in table 5.6. Table 5.6 shows the calculated conductivity and sheet resistivity of Nickel doped tin oxide. It was noticed that sheet resistivity reduced with doping concentration increase in tin oxide from 46.84 Ωcm to 23.53 Ωcm.

The sheet resistivity for Nickel doped Tin oxide obtained is in the range of a semiconductor at room temperature which according to Shimura (1989) ranges from 10^{-1} to 10^{9} Ωcm. This could be correlated to upsurge carrier concentration and carrier mobility which is associated with the film.

Table 5.6: The variation of sheet resistivity and conductivity with Nickel concentration in Tin oxide.

% Nickel concentration	Sheet resistivity ($\pm$ 0.005 Ωcm) x 10^1 .	Conductivity ($\pm$ 0.005)Ωcm^{-1} x 10^{-2}
0	4.684	2.135
2	4.333	2.308
4	3.943	2.536
6	2.893	3.457
8	2.478	4.036
10	2.353	4.250

Figure 5.20 shows a general drop in resistivity as the doping level increases. This may be correlated to the circumstance that SnO_2 are normally recompensed by the creation of oxygen vacancies by the dopants of Ni^{+2} which are acceptors. Therefore, the rise in dopant concentration gives rise to free electrons density hence conductivity. Nonetheless, the replacement of Sn^{+4} with Ni^{+2} can occur to a specific limit. When this limit is exceeded due to introduction of extra Ni^{+2}, the excess Ni^{+2} which cannot replace Sn^{+4} further will separate to grain boundary interface. Hence, the separation of Ni^{+2} blocks the accumulation and flow of electrons together with other defects and then lowers its conductivity (Azam *et al*., 2010).

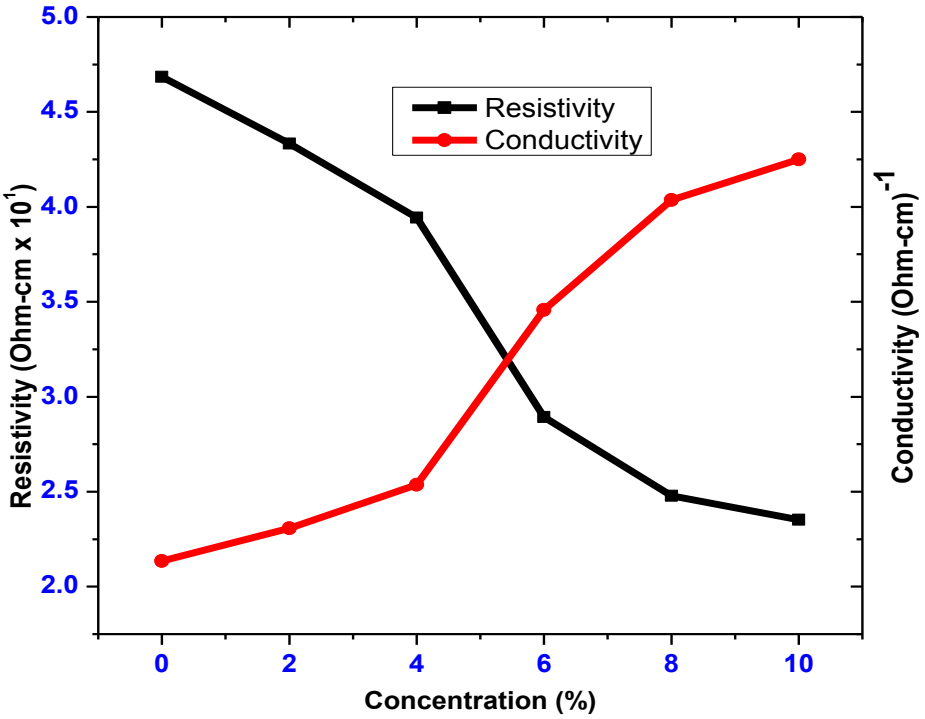

Figure 5.20: Variation of sheet resistivity and conductivity at different Nickel concentration.

5.4 Fabrication and characterization of SnSe-SnO_2: Ni p-n junction

Fabrication of the p-n junction solar cell with glass/SnO_2: Ni/SnSe/Al was achieved in stages**.** The SnO_2: Ni film which acts as a window layer and in this case n type layer was coated onto a glass substrate and an absorber thin film of SnSe coated onto SnO_2: Ni on the same substrate to make a p-type layer. Fabrication was completed by deposition of Aluminium as rare contact on SnSe film to complete the solar cell. 2% Ni doped SnO_2 had the highest transmittance within the visible region of the electromagnetic spectrum as shown in figure 5.13. It was hence chosen as a window layer for fabricating SnSe-SnO_2: Ni solar cell and had relatively low electrical resistance. A SnSe film exhibited high absorbance, low transmittance and low reflectance within the visible region as shown in figure 5.6 hence was used as an absorber layer.

In SnSe-SnO_2: Ni solar cell fabrication, low absorption, high transmittance and low reflectance are some of the optical properties which are taken into account when choosing a window layer, while high absorption coefficient, low transmittance and low reflectance are needed for an

absorber layer for PV applications.

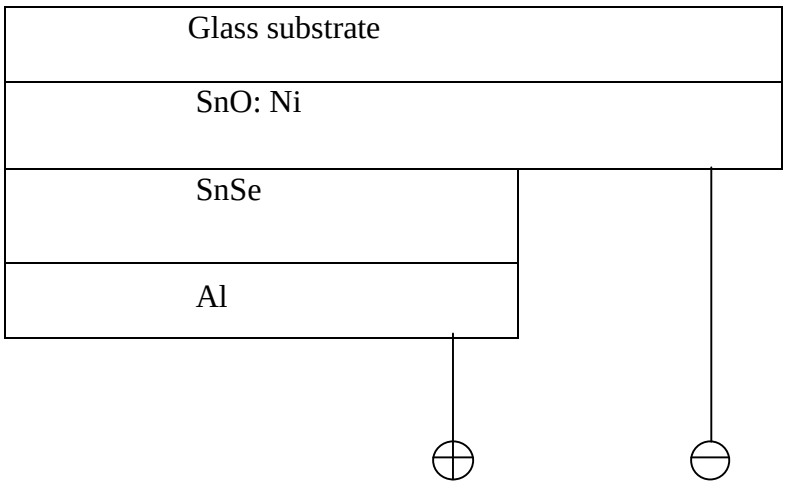

Figure 5.21: Fabricated SnO_2: Ni/SnSe/Al p-n junction solar cell schematic diagram.

Data that was used to plot the I-V characteristics was extracted using a solar cell simulator fitted with dichroic reflector. From the I-V characteristic, short circuit current and the open circuit voltage values were achieved. When current is not flowing through the cell open circuit voltage (V_{OC}) is obtained, V (at I = 0) = V_{OC}. When the impedance is low the short circuit current (I_{SC}) is obtained which corresponds to the short circuit state and is attained when the voltage same as zero. I (at V=0) = I_{SC}. In the power quadrant, maximum current is attained known as $I_{SC,}$ which occurs at the starting point of the forward-bias sweep. The I-V characteristic of the fabricated P-N junction solar cell is shown figure 5.22 below.

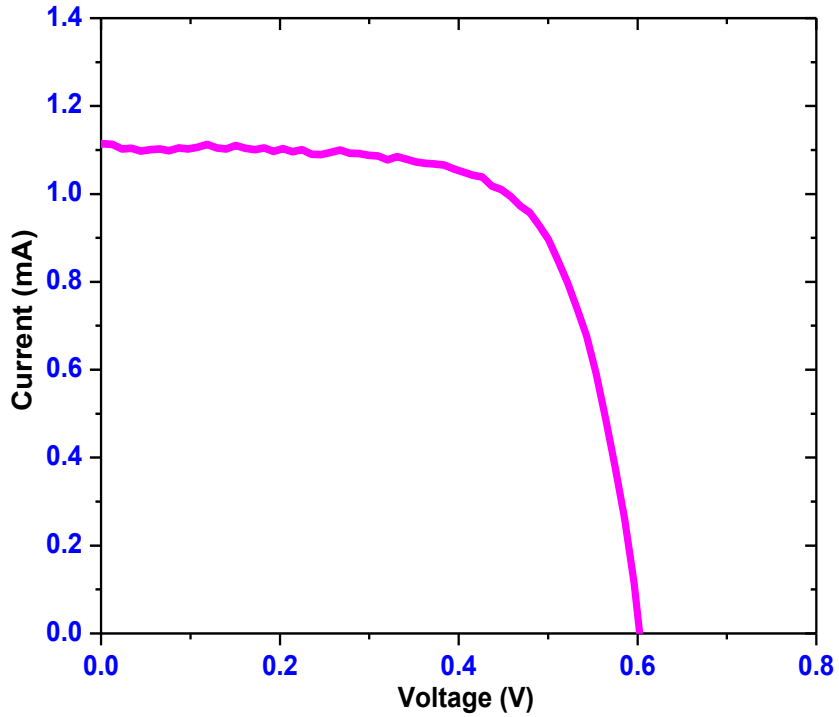

Figure 5.22: Simulated I-V characteristic of the fabricated SnSe-SnO2: Ni p-n heterojunction solar cell.

Due to the presence of impurities that occurs during deposition process, back aluminium contact resistance and electron hole recombination, the value of short circuit current is usually low which causes the solar cell experience somewhat higher resistance to the flow of charges. The measurement of the quality of a solar cell eventually obtained by squareness of current-voltage curve is the Fill factor (FF). This is done by relating the maximum power to the theoretical power (P_T) that would be the result at short circuit current and open circuit voltage altogether. The fabricated solar cell of an area $4cm^2$ gave the following I-V characteristic from the results owing to the solar cell simulator.

Table 5.7: Parameters of SnSe- SnO_2: Ni p-n junction

The parameters of solar cell obtained are given are shown on the table 5.5

PARAMETER	VALUE
V_{oc}	607 mV
V_{max}	479 mV
I_{sc}	1.118 mA
I_{max}	0.9615 mA
Fill factor (FF)	0.6792
Efficiency (η)	0.4609%

The V_{OC} which is the open circuit voltage, was 0.607V and I_{SC} which is the short circuit current, was 1.118 mA/cm^2. The fill factor and conversion efficiency of the assembled solar cell were achieved using equations 3.21 and 3.23 respectively. Fill factor estimate was seen to be 0.6792. Using incident power of 100W from the solar simulator's illuminated on the fabricated solar cell, the conversion efficiency (η) which is the ratio of P_{out}, the electrical power output compared to P_{in}, the solar power input into the solar cell was attained as 0.4609%.

CHAPTER 6

CONCLUSION AND RECOMMENDATIONS

6.1 Conclusion

Thin films of Sn_xSe_y has shown transmittance of below 65% in the visible range (400nm-780nm). Transmittance decreased with increase in selenium ratios and after attaining a ratio of 1:1 it again increases. A sample of $Sn:Se_{1.0}$ had the lowest transmittance of 44.3%. This could be due to its low band gap compared to other samples. The average reflectance within the visible region was less than 10% for all the tin-selenide samples, indicating that the film had high absorption. This low reflectance could be associated with the surface roughness which caused diffused reflection. A sample of Sn:Se had the highest absorbance of 46.46%.

The average absorption coefficient within the visible range for all the samples of Sn_xSe_y increases with increasing tin-selenide ratio up to a ratio 1:1 and then decreases. The average absorption coefficient of $> 10^5$ cm^{-1} were obtained for Sn:Se that made it an acceptable material for making a good p type layer for a solar cells. A sample ratio of 1:1 of SnSe has the highest refractive index implying that it is a good absorber material and this is because the radiation takes a longer time to go through the film. SnSe film of ratio 1:1 had highest extinction coefficient implying that its rate of absorption was the best.

The optical band gap energy of Sn_xSe_y lies between 1.39-2.23±0.05 eV with the Sn:Se ratio of 1:1 having the lowest band gap energy. Sheet resistivity of Sn_xSe_y reduced with increase of selenium in tin from 39.32 Ωcm to a minimum of 28.82 Ωcm. Conductivity increases, due to the rise in carrier mobility a behavior attributed to the enlargement of the grain size.

The optical transmittance of SnO_2 and Nickel doped SnO_2 was found to be above 75% in the VIS and NIR region. The 2% Nickel doped sample depicted a somewhat higher transmittance

comparing with other samples making it a good material for a window layer. High transmittance is associated with the wide band gap of the film compared to other samples. Reflectance of SnO_2 and Nickel doped SnO_2 ranged between 8-10% in the infra-red region, the ultra violet and visible range of the electromagnetic spectrum. This low reflectance was associated to the surface roughness which caused diffused reflection.

The refractive index decreased with 2% Nickel showing the least value and then increasing. This means the photons travels faster through that film faster hence absorption is minimal. This is what makes it to have high transmittance. Average absorption coefficient was lowest for film with 2% Nickel doping concentration within the visible range. This indicated that the film is good for a window layer. The average extinction coefficient within the visible range was below 0.2 for all the samples of doped and un doped Tin Oxide. A film with the lowest extinction coefficient in the visible region was the 2% doped film making it a good n type layer

The calculation of SnO_2: Ni band gap has been found to be between 3.68eV and 3.75eV. SnO_2: Ni of doping concentration 2 % had the highest band gap of 3.75 among the other samples. Sheet resistance for SnO_2 reduced with increase in Nickel doping to a minimum from 46.84 Ω-cm to 23.53 Ω-cm as doping levels for as prepared samples increased from 0-10%.

For the absorber layer, the solar cell was assembled using Sn:Se ratio of 1:1 while 2% Nickel doping on SnO_2: Ni was used as a window layer, since it portrayed the best trend within visible range.

The I-V characteristics analysis offered open circuit voltage V_{oc} = 0.607V, short circuit current I_{sc} of 1.118mA/cm^2, fill factor=0.6792 with efficiency η of 0.4606%.

The efficiency of 0.4609% was quite low in comparison to Beyond 11% efficiency: Characterization of state of the art $Cu_2ZnSn(S,Se)_4$ solar cells. Recent performance enhancement in $Cu_2ZnSn(S_{1-x}Se_x)$(CZTSSe) devices, in which indium and gallium from

CIGSSe are replaced by a more abundant and lower cost Zinc and tin have efficiencies of over 11%. Evidence has shown moderate thickness of the absorber layer CZTSSe (about 200 nm thickness) and a band gaps in the range 1.08 – 1.12 eV. A Ni-AL collection grid and ~ 110 nm thick MgF_2 antireflection coating were deposited. Scanning electron Microscopy (SEM) was conducted. Scanning transmission electron microscopy (STEM) images were taken. (Todorov T. K. *et al*., 2013)

CZTSSe (Kesterite – type crystal structure) was reported in 1996 to have an efficiency of 0.66%. Subsequent optimization using both evaporation and sputtering led to performance of 6.7 % in 2008. Hydrazine – based deposition process was announced with efficiency of 9.7% which further improved to 10.1 % in 2011. The highest certified power conversion efficiency at the 11.1 % level was reported in 2012. (Todorov T. K. *et al*., 2013)

6.2 Recommendations for further work

Recommendation for more research on a treated solar cell is made.

An applicable of anti-reflective coating (ARC) is recommended so as to compensate for reflection losses of thin film of SnSe/ SnO_2: Ni solar cell.

Structural analysis of the thin film should be undertaken to access the device morphology to ascertain whether interface defects and optical properties would be reduced during deposition of SnO_2: Ni thin films. Optimization of film thickness and deposition temperature of SnSe/ SnO_2: Ni solar cell is also recommended.

REFERENCES

Agumba, J. O. (2010). Design and fabrication of a simple four point probe system for electrical characterization of thin films. *MSc Thesis, Department of Physics.Kenyatta University.American Journal of Materials Science,* **2**: 41- 45.

Ajimsha, R.S., Das A.K., Singh, B.N., Misra, P., Kukreja, L.M. (2011). Correlation between electrical and optical properties of Cr:ZnO thin films grown by pulsed laser deposition. *Laser Materials Processing Division, Raja Ramanna Centre for Advanced Technology, India*

Andreev, V.M., Grilikhes, V. A. and Rumyantsev, V .D (1997). Photovoltaic conversion of concentration sunlight. *(Monograph), John wiley & sons.*

Aruchamy, A., (1992). Photo electrochemistry and Photovoltaic of Layered Semiconductor. *Kluwer Academic Publishers, Dordrecht.*

Azam, A., Arham, S. A., Shahnawaze, A., Muhamed, S. M. and Alim, H. N. (2010). Study of electrical properties of nickel doped SnO_2 ceramic nanoparticles. *Journal of Alloys and Compound*, **506**: 237-242

Bindu, K. & Nair, P. (2004). Semiconductor tin selenide thin films prepared by heating Se-Sn. *Journal of Semiconductor Science and Technology* **19**: 1348-1353.

Born, M. and Wolf, E. (1975). Principles of Optics. *Pergamon, Oxford.*

Brennan, K.F. (1999). The Physics of Semiconductors with applications to Optoelectronic Devices. *Cambridge University Press, London.*

Brown, M. & Jakeman, F. (1996). Theory of four point probe technique as applied to film layers on conducting substrates. *British Journal of applied Physics*. **17**: 1146-1149. *Chalcogenide Letters,* **7**: 211- 216.

Charles, M. O. O., Okumu, J., Njoroge, W. K. (2011). Characterization of Sn_xSe_y-ZnO:Al p-n junction for solar cell applications. *Msc Thesis Kenyatta University.*

Chopra, K.L. & Krieger, R.E. (1969). Thin Film Phenomena. Huntington, New York.

Chuah, L. S., Yaacob, M. S., Hassan Z. (2012). Low temperature synthesis of Ni-doped SnO2 thin films by spin coating route. *Physics Section, School of Distance Education, Universiti Sains Malaysia*, 6 (**1-2)**: 149 – 153.

Chung, K. M., Wamwangi, D. and Woda, M. (2008). Investigation of SnSe, $SnSe_2$, and Sn_2Se_3 alloys for phase change memory applications. *Journal of Applied Physics* **103**: 083523.Delhi.

Fahrenbruch, A. L. & Bube, R. H. (1983). Fundamentals of Solar cells. *New York Academic Press.*

Gall, S., Becker, C., Conrad, E., Dogan, P., Fenske, F., Gorka, B., Lee, K.Y., Rau, B., Ruske, F. and Rech, B. (2009). Polycrystalline silicon thin-film solar cells on glass. *Solar Energy Materials and Solar Cells,* **93:** 1004–1008.

Ghosh, D. S., Chen, T. L., Krautz, D., Cheylen, and Pruneri, V. (2011). Environmentally stable Al-doped ZnO transparent electrode for organic optoelectronic devices.

Gowri, S. (2003). Characterization of Cadmium Zinc Telluride Solar Cells. *Msc Thesis. University of South Florida, College of Engineering: Department of Electrical Engineering. New york.*

Green, M. A. (2002). "Third generation photovoltaic solar cells for 2020 and beyond", *Low – dimensional Systems and Nanostructures* **14:** 65-67.

Gullen, C., Montero, J., Herrero, J. (2011). Characteristics of SnSe and $SnSe_2$ thin films grown onto polycrystalline SnO_2-coated glass substrates. *Physics Status Solids* **208:** 679

Hema, G., Naveen, J. and Uthanna, S. (2007). Preparation and characterization of flash evaporated tin selenide thin films. *Journal of Crystal Growth*, **306**: 68-74

Jebbari, N., Kamoun, N. and Bennaceur, R. (2010). Effect of $SnCl_4$ concentration on F: SnO_2, deposited by chemical spray pyrolysis. *In the proceedings of International Renewable Energy Congress, Souse, Tunis* **2:** 276-279.

Jeewan, S. G., Singh, A., Thakur, G.S., Saini, N., Goyal, and Tripathi,S.K. (2005). Preparation and characterization of SnSe nanocrystalline thin flms. *Journal of Optoelectronics and Advanced Materials;* **7**, *2085*.

Jorge S. N. R., Aaron S., Juarez D., Martinez-Escobar, Manoj R. (2015). Structural and electrical characterization of snse and snse2 thin films deposited by Ultrasonic spray pyrolysis.

Kekuda, Nagaraju, and Krupanidhi, S. B. (2006). Temperature dependent transport properties of $CuInSe_2$–ZnO Heterostructure Solar cell. *Journal of Physics and Chemistry of Solids*, **67 (8)**: 1636-1642. ISSN 0022-3697

Korotcenkov, G., Brinzari, V., Boris, I. (2008). (Cu, Fe, Co, or Ni)-doped tin dioxide films deposited by spray pyrolysis: doping influence on film morphology. *Journal of Mater Science: Mater Electron,* **43**:2761–2770.

Kumar, N. (2010). Influence of the substrate temperature on the structural, optical and electrical properties of tin selenide thin films deposited by thermal evaporation method. *Crystal Research Technology,* **45**: 53-58.

Kumar, N. (2012). Effect of Film Thickness on Optical Properties of Tin Selenide Thin Films Prepared by Thermal Evaporation for Photovoltaic Applications. *American Journal of Materials Science*, **2**: 41-45

Kumar, N., Sharma, V., Parihar, U., Sachdeva1, R., Padha, N. and Panchal, C. (2011). Structure, optical and electrical characterization of tin selenide thin films deposited at room temperature using thermal evaporation method. *Nano- Electronic Physics,* **3**: 117-126.

Kuo-Jui, H. (2010). Electron-Reflector strategy for CdTe thin-film solar cells. *PhD Thesis. Colorado State University, Department of Physics, New york.*

Kuppan, M., Kaleemulla, S., Madhusudhana, R. N., Sai Krishna N., Rigana, B. M., and Shobana, M. (2014). Structural and Magnetic Properties of Ni Doped SnO_2. *Research Article.*

Lawrence, K.M., (2011). Characterization of SnSe/ZnO:Sn P-N junction for solar cell application. M.sc. thesis. *Kenyatta University. Kenya*

Lindgren, T., Larsson, M. and Lindquist, S. (2002). Solar Energy Materials. *Journal of Solar*

Cells, **73**: 377-377.

Mariappan, R., Ragavenda, M., and Gowrisankar, G., (2010). Growth and characterization of SnSe thin films prepared by spray pyrolysis technique.

Markvat, T. (1998). Solar Electricity. *John Wiley & Sons. New York,* **3-4:** 34-35.

Martinez-Escober, Manoj, R., Sanchez-Juarez, A. and Jorge, S. N.R. (2013). Optical and electrical properties of $SnSe_2$ and SnSe thin films prepared by spray pyrolysis. *Thin Solid Films.* Vol **535**, Pg 390–393.

Mohd, A., Syafiq, Y., Zainal, T. and Wan, Y. (2011). Annealing and light effect on structural and electrical properties of thermally evaporated Cu_2SnSe_3 thin films. *Chemical Engineering and Materials Science,* **2:** 103-109.

Mohsen, D. & Mousa, A. (2012). Experimental study of structural and optical band gap of nickel doped tin oxide nanoparticles. *International Journal of Physical Sciences*. **7(37)**: 5415-5420.

Nyakundi, M.E. (2014). Characterization of snse-cdo:sn p-n junction for solar cell applications. *M.Sc. Thesis. Kenyatta University. Kenya*.

O"Leary, J., Johnsons, R. and Lim, P. (1997). Thin film Physical models. *Journal of Applied Physics,* **8** (7), 12-87.

Okereke, N.A. and Ekpunobi, A.J. (2012). Spectroscopic studies on lead selenide (pbse) and tin selenide(snse) thin films. *Journal of Optoelectronics and Biomedical Materials,* **3**: 69-74.

Oztas, M., Bedir, M., Bakkaloglu, O.F. and Ormanc, R. (2004). Effect of Zn:Se ratio on the properties of sprayed ZnSe Thin Films. *University of Gaziantep, Department of Engineering Physics* 27310-Gaziantep, Turkey.

Pathinettam, P.D., Marikani, A. and Murali, K.R. (2000). Crystal Research Technology. *Material Science,* **35**: 949-949.

Pirog, R. (2005). World Oil Demand and its Effect on Oil Prices. *Congressional Research Service Report.*

Porotmans, J. & Arkhipov, V. (2006). *Thin film solar cells fabrication, characterization and applications*. John Wiley and Sons. Chinchester.

Ranjdar, M. & Ali, B. (2006). Optical Properties of Thin Film. Ministry of Higher Education Sulaimani University College of Science Physics Department, Iraq.

Serhan, A. A. (2005). Preparation and Characterization of Chlorine doped Cadmium Sulphide (Cds:Cl) thin films and their applications in solar cells. *Msc Thesis. King Saud University, College of Science: Department of Physics and Astronomy.*

Sharma, J., Singh, G., Thakur, A., Saini, G., Goyal, N. and Tripathi, K. (2007). Preparation and Characterization of SnSe nanocrystalline thin films. *Journal of Optoelectronics and Advanced Materials* **7:** 2085-2094.

Shimura, F. (1989). Basic semiconductor physics. In Semiconductor Silicon Crystal Technology, edited by Shimura, F. San Diego: *Academic Press*. p. 82.

Shishiyanu, S. T., Shishiyanu, T. S. Lupan, O. I. (2004). Sensing characteristics of tin-doped ZnO thin films as NO2 gas sensor. *Department of Microelectronics and Semiconductor Devices, Technical University of Moldova.*

Singh, J. (2003). Electronic and Optoelectronic properties of semiconductor structures. Cambridge University Press. *Edinburgh UK.*

Stefano, G., Anabel, R., Luis, M., Paolo, V., Federico, L., Sarah, B., Alerio, P. (2007). Ultra-thin nickel transparent electrodes. *Journal of Mater Science: Mater Electron*, **20**:S181–S184.

Suhail, M. H., Abdullah, M. M. and Abbas, S. L. (2012). Structural, Electrical and Photoluminescence properties of In_2O_3 – Doped SnO_2. *Journal of Chemical, Biological and Physical Science* **2:** 1963-1973.

Sumbit, C. (2008). Studies of ZnSe and Indium Tin Oxide based thin film schottky barriers and heterojunctions for their electrical and optical properties. *PhD Thesis. Gauhati University, Faculty of science India.*

Swanson, R. M. (2000). The Promise of Concentrators. *Progress in Photovoltaics: Research. Applications,* **8**: 93–111.

Sze, S.M. (1981). Physics of semiconductor devices. *John wiley and sons. New York*, 742.

Theiss, W. in: W. Theiss (Ed.), (2001). Scout Thin Film Analysis Software Handbook, Hard and Software,Aachen, Germany, *www.mtheiss.com*, pp: 54-57.

Todorov, T. K., Jiang, T., Santanu B., Oki G., Tayfun G., Yu, Z., and David B. M. (2013). Beyond 11% Efficiency: Characteristics of State-of-the-Art $Cu_2ZnSn(S,Se)_4$ Solar Cells. *Advance Energy Mater. 3,* 34–38.

Toshiyuki, Y., Jiro, M. and Akira, Y. (1991). Thin films of $CuInSe_2$ prepared by RF sputtering from various compositional powder targets: *Solar Energy materials and solar cells* **27:** 25-35.

Vadivel, K., Arivazhagan, V. and Rajesh, S. (2011). Room Temperature Ferromagnetism of Ni Implanted SnO2 Nanopowders. *International Journal of Applied Engineering Research.***1**:4.

Waita, S.M., (2008). Dye sensitized TiO2 solar cells. *Phd. Thesis, university of Nairobi*.

Yadav, A. A., Masumdar, E. U., Moholkar, A. V., Rajpure, K. Y. and Bhosale, C. H. (2008). Gas Sensing of Fluorine Doped Tin Oxide Thin Films Prepared by Spray Pyrolysis. *Journal of Sensors & Transducers,* **92:** 55-60.

Zainal, Z., Nagalingam, S., Kassim, A., Hussein, M. and Yunus, W. (2003). Tin Selenide thin films prepared through combination of chemical precipitation and vacuum evaporation technique. *Material Science,* **21**: 225-233.

Zheng, B.J., Lian, J.S., Zhao, L. and Jiang, Q. (2011). Optical and electrical properties of Sn-doped thin films obtained by Pulse Laser deposition. *Vacuum Technology,* **85**: 861-865.

Zhou, D. (2008). Light-trapping enhancement in thin film solar cells with photonic crystals. *Msc Thesis. Iowa State University. Ames, Iowa.*